Downloaded from orbit.dtu.dk on: Apr 20, 2024

DTU Library

Physical routes for the synthesis of kesterite

Topical Review

Ratz, T.; Brammertz, G.; Caballero, R.; León, M.; Canulescu, Stela; Schou, J.; Gütay, L.; Pareek, D.; Taskesen, T.; Kim, D.-H

Total number of authors:
19

Published in:
Journal of Physics: Energy

Link to article, DOI:
10.1088/2515-7655/ab281c

Publication date:
2019

Document Version
Publisher's PDF, also known as Version of record

Link back to DTU Orbit

Citation (APA):
Ratz, T., Brammertz, G., Caballero, R., León, M., Canulescu, S., Schou, J., Gütay, L., Pareek, D., Taskesen, T., Kim, D. -H., Kang, J. -K., Malerba, C., Redinger, A., Saucedo, E., Shin, B., Tampo, H., Timmo, K., Nguyen, N. D., & Vermang, B. (2019). Physical routes for the synthesis of kesterite: Topical Review. *Journal of Physics: Energy*, *1*(4), Article 042003. https://doi.org/10.1088/2515-7655/ab281c

General rights
Copyright and moral rights for the publications made accessible in the public portal are retained by the authors and/or other copyright owners and it is a condition of accessing publications that users recognise and abide by the legal requirements associated with these rights.

- Users may download and print one copy of any publication from the public portal for the purpose of private study or research.
- You may not further distribute the material or use it for any profit-making activity or commercial gain
- You may freely distribute the URL identifying the publication in the public portal

If you believe that this document breaches copyright please contact us providing details, and we will remove access to the work immediately and investigate your claim.

JPhys Energy

TOPICAL REVIEW • OPEN ACCESS

Physical routes for the synthesis of kesterite

To cite this article: T Ratz *et al* 2019 *J. Phys. Energy* **1** 042003

View the article online for updates and enhancements.

This content was downloaded from IP address 130.226.56.2 on 04/10/2019 at 12:48

JPhys Energy

OPEN ACCESS

RECEIVED
12 April 2019

REVISED
29 May 2019

ACCEPTED FOR PUBLICATION
10 June 2019

PUBLISHED
12 September 2019

Original content from this work may be used under the terms of the Creative Commons Attribution 3.0 licence.

Any further distribution of this work must maintain attribution to the author(s) and the title of the work, journal citation and DOI.

TOPICAL REVIEW

Physical routes for the synthesis of kesterite

T Ratz[1,2], G Brammertz[3], R Caballero[4], M León[4], S Canulescu[5], J Schou[5], L Gütay[6], D Pareek[6], T Taskesen[6], D-H Kim[7], J-K Kang[7], C Malerba[8], A Redinger[9], E Saucedo[10], B Shin[11], H Tampo[12], K Timmo[13], N D Nguyen[1] and B Vermang[2,14,15]

[1] CESAM—Q-MAT—Solid State Physics, Interfaces and Nanostructures, Physics Institute B5a, Allée du Six Août 19, B-4000 Liege, Belgium
[2] Institute for Material Research (IMO), Hasselt University, Agoralaan gebouw H, B-3590 Diepenbeek, Belgium
[3] IMEC division IMOMEC—partner in Solliance, Wetenschapspark 1, B-3590 Diepenbeek, Belgium
[4] Universidad Autonoma de Madrid, Departamento de Fisica Aplicada, C/Francisco Tomaas y Valiente 7, E-28049 Madrid, Spain
[5] DTU Fotonik, Technical University of Denmark, DK-4000 Roskilde, Denmark
[6] Abteilung Energie-und Halbleiterforschung (EHF), Institut für Physik, Carl von Ossietzky Universität Oldenburg, Germany
[7] Convergence Research Center for Solar Energy, Daegu Gyeongbuk Institute of Science and Technology (DGIST), Daegu 42988, Republic of Korea
[8] ENEA,Casaccia Research Center, via Anguillarese 301, I-00123 Roma, Italy
[9] Scanning Probe Microscopy Laboratory, University of Luxembourg 162a, Avenue de la Faïencerie, L-1511, Luxembourg
[10] Catalonia Institute for Energy Research (IREC), Jardins de les Dones de Negre 1 2pl., E-08930 Sant Adrià del Besòs-Barcelona, Spain
[11] Department of Materials Science and Engineering, Korea Advanced Institute of Science and Technology (KAIST), 291 Daehak-ro, Yuseong-gu, Daejeon 34141, Republic of Korea
[12] National Institute of Advanced Industrial Science and Technology (AIST), Research Center for Photovoltaics, Tsukuba, Ibaraki 305-8568, Japan
[13] Department of Materials and Environmental Technology, Tallinn University of Technology, Ehitajate tee 5, 19086 Tallinn, Estonia
[14] Imec division IMOMEC (partner in Solliance), Wetenschapspark 1, B-3590 Diepenbeek, Belgium
[15] Energyville, Thor Park 8320, B-3600 Genk, Belgium

E-mail: thomas.ratz@uliege.be

Keywords: kesterite, earth-abundant materials, absorber layer, thin film solar cell, physical vapor deposition

Abstract

This paper provides an overview of the physical vapor technologies used to synthesize $Cu_2ZnSn(S,Se)_4$ thin films as absorber layers for photovoltaic applications. Through the years, CZT(S,Se) thin films have been fabricated using sequential stacking or co-sputtering of precursors as well as using sequential or co-evaporation of elemental sources, leading to high-efficient solar cells. In addition, pulsed laser deposition of composite targets and monograin growth by the molten salt method were developed as alternative methods for kesterite layers deposition. This review presents the growing increase of the kesterite-based solar cell efficiencies achieved over the recent years. A historical description of the main issues limiting this efficiency and of the experimental pathways designed to prevent or limit these issues is provided and discussed as well. A final section is dedicated to the description of promising process steps aiming at further improvements of solar cell efficiency, such as alkali doping and bandgap grading.

1. Introduction

Research on renewable energy sources and more precisely photovoltaic (PV) solar cells takes place in a world-wide effort to meet the growing energy demand and to tackle climate change. The use of chalcogenide materials such as $Cu(In,Ga)(S,Se)_2$ as absorber layer in solar cells has drawn a major attention in the scientific community over the past 40 years, with a world record efficiency of 23.35% achieved in January 2019 [1]. More recently, a family of related materials, i.e. kesterite materials, has enabled the achievement of efficiencies within the range of 10%–12.6% [2–10]. This material family is revealed as a promising candidate for low-cost, high-efficiency and earth-abundant solar cells. Since 2011, the European Commission (EC) has expressed its ambition for 'Critical Raw Materials' (CRM) free technologies. A reviewed list of CRMs including Ga and In was published by the EC in 2017 [11]. As a consequence, in order to answer these current issues and address upcoming requests, an

© 2019 The Author(s). Published by IOP Publishing Ltd

intensive research on $Cu_2ZnSn(S,Se)_4$ (CZT(S,Se)) kesterite compounds as CRM-free absorber layers for PV applications is essential. This article aims at establishing a complete overview of the physical routes used for the synthesis of kesterite thin films as absorber layers in solar cells. The following sections are devoted to that objective and will take on the main issues which have been raised so far as well as how the processes have evolved through the years to meet the requirements of the market. Some major advancements in terms of deposition or post-deposition treatments are introduced. Advantages and drawbacks of each of the physical methods presented in this review are described in detail and compared to other physical or chemical synthesis routes.

2. Physical routes: status overview

We performed an extensive identification of the common processes and methods used for the synthesis of kesterite thin films or for the design of solar cell devices. In order to avoid unnecessary repetitions along this paper, this section first explains these well-known and commonly used experimental processes and methods. Historically, based on the similarities between kesterite and chalcopyrite compounds, the standard device structure adopted for $Cu(In,Ga)(S,Se)_2$ (CIGSSe) was directly extended to CZTSSe, by simply replacing the CIGSSe absorber layer with a p-type CZTSSe thin film. CZTSSe solar cells are then typically produced using a soda-lime glass (SLG) substrate coated with a sputtered Mo layer acting as rear metallic contact. Typical sputter-deposited Mo layer thickness is around 500 nm up to 1 μm [12]. The kesterite absorber is then deposited onto the Mo layer.

The fabrication of this absorber consists in the deposition of a precursor layer via a physical or a chemical route, which is then annealed in a reactive atmosphere containing either S (sulfurization) or Se (selenization). As a common result of the reactive annealing, a thin $Mo(S,Se)_2$ layer is naturally formed at the CZTSSe/Mo interface, between a few nanometers up to a few microns thick, depending on the synthesis conditions and the Mo properties, due to a partial selenization or sulfurization of the back contact. This $Mo(S,Se)_2$ intermediate layer is also typically formed in the CIG(S,Se) technology, and all evidences indicate that this p-doped layer helps to improve the ohmic character of the back contact [12, 13]. After the absorber deposition, chemical treatments can be applied to the surface in order to remove secondary phases and/or to prepare the surface for the subsequent PN junction formation. Details related to such aspects are provided in another contribution of this journal issue.

Cadmium sulfide (CdS) is normally used as the buffer (n-type) layer of the PN junction. This layer is most commonly deposited by chemical bath deposition with a typical thickness of the order of 50–100 nm. The so-called window layer consists of an intrinsic ZnO and a transparent conducting oxide (TCO) layer (indium tin oxide or aluminum zinc oxide) both deposited by sputtering with a thickness of 50–100 nm and 200–400 nm respectively. Finally, a metallic Al, Ni or Ni/Al grid is deposited as front contact of the cell. Ultimately, the complete structure of the device is Al-Ni/TCO/ZnO/CdS/CZT(S,Se)/$Mo(S,Se)_2$/Mo/SLG. Sometimes, an anti-reflective (AR) coating (usually MgF_2) is deposited on the top of the device.

Additionally, we must take into account that these established deposition processes are not suitable for the monograin growth which is a specific physical route for the synthesis of kesterite type crystalline powders. The details of this physical route will be presented at a later stage. Having the general structure of kesterite solar cells in mind, three types of different physical routes used for the synthesis of kesterite thin film as absorber layer are discussed in this paper, leading to the organization of this review as follows:

- One-step processes are described in section 2.1,
- two-step processes are presented in section 2.2, with discussion on the particular technologies related to:

sequential evaporation and co-evaporation,

sequential sputtering and co-sputtering deposition,

pulsed laser deposition (PLD),

- monograin growth process is finally shown in section 2.3.

Cell efficiencies for CZTS- and CZTSe-based cells obtained using the previously presented physical routes for the synthesis of the kesterite absorber layers are presented in tables 1 and 2, respectively. The benchmark performances for the different physical routes are given using the following PV parameters: the bandgap energy E_g [eV], the efficiency η [%], the open-circuit voltage V_{OC} [mV], the short-circuit current density J_{SC} [mA cm^{-2}], the fill factor FF [%] and the area A [cm^2] for each absorber layer synthetized by different groups. As the purpose of this paper is to highlight the impact of the deposition parameters of the absorber layer on the device efficiency, additional information has been added to this overview table, such as the substrate temperature during the deposition T_S [°C] and the annealing

Table 1. Overview table of the CZTS-based cell efficiencies focusing on the absorber layers grown by different physical routes. Substrate temperature T_S, annealing temperature T_A, annealing atmosphere (Atm.), post-deposition annealing (PDA), anti-reflective coating (AR), bandgap energy E_g [eV], efficiency η [%], open-circuit voltage V_{OC} [mV], short-circuit current density J_{SC} [mA cm^{-2}], fill factor FF [%], area A [cm^2].

Route (Year)	T_S [°C]	T_A [°C]	Atm.	Notes	Buffer Type	PDA	AR	E_g [eV]	η [%]	V_{OC} [mV]	J_{SC} [mA cm^{-2}]	FF [%]	A [cm^2]	Institution References
Co-Sputt. (2008)	RT	580	H_2S, N_2	2.2 μm-**CZTS**: Cu, SnS, ZnS, soaked in DIW	CdS	No	No	/	**6.8**	610	17.9	62	0.15	NNTC [15]
Co-Evap. (2013)	~150	570	S_2,N_2	600 nm-**CZTS**: Cu, Zn, Sn, S (hot plate; 5min)	CdS	No	MgF_2	1.45	**8.4**	661	19.5	65.8	N.D.	IBM [16]
Seq. Evap. (2013)	/	/	S	**CZTS**: Submodule (7 cells)	In_2S_3/ CdS	/	Yes	/	**9.2**	708	21.6	60.1	14	Solar frontier [17]
Co-Sputt. (2013)	180	560	Ar, S	**CZTS**:Cu/Sn, Zn in H_2S reactive atm., KCN etched	CdS	/	No	/	**7.9**	667	19.6	60.0	/	Uppsala [18]
Seq.Sputt. (2015)	RT	570	S	~500 nm-**CZTS**:Cu/SnS/ZnS/Mo	CdS	No	No	1.50	**7.5**	632	19.2	61.6	0.4	DGIST [19]
Monograin (2015)	/	740	S	**CZTS**:KCN etched	CdS	No	No	1.53	**9.4** (EA)	713	21.24	62	0.04	Taltech [20]
Co-Sputt. (2016)	RT	560	S	~900 nm-**CZTS**:Cu/ZnS/SnS/Mo	$Zn_{0.35}$ $Cd_{0.65}S$	No	No	1.50	**9.2**	748	19.5	63.2	0.4	UNSW [21]
Co-Sputt. (2016)	RT-250	250-510	N_2, H_2S	1 μm-**CZTS**:SnS_2, ZnS, Cu	CdS	No	MgF_2	1.4	**8.6**	625	21.2	65.1	0.5	SIAT [22]
Co-Sputt. (2017)	RT	580	S	**CZTS**:CuS,ZnS and SnS, ZTO ALD (145 °C)	(Zn,Sn)O	CZTS	MgF_2	1.50	**9.0**	679	21.6	61.4	0.5	Uppsala [23]
Co-Sputt. (2017)	RT	570	S	900 nm-**CZTS**:Cu,ZnS,SnS	CdS	On cell	Yes	1.5	**7.9**	642	19.3	64	0.1	ENEA [24]
PLD (2017)	RT	560	S,SnS	<450 nm- **CZTS**:2CuS:ZnS:SnS	CdS	No	MgF_2	1.53	**5.2**	616	17.6	47.9	0.21	DTU [25]
Monograin (2017)	/	740	S	**CZTS**:PA at 150 °C (4h), KCN etched	CdS	CZTS	No	1.55	**9.1** (EA)	759	19	63	0.04	Taltech [26]
Co-Sputt. (2018)	RT	560	SnS, S	**CZTS**:Cu/ZnS/SnS/ Al_2O_3/Mo,	CdS	CZTS	Yes	1.5	**11.0**	731	21.74	69.3	0.234	UNSW [5]
PLD (2019)	/	/	/	**CZTS** Oxide target	/	/	/	/	**5.4**	673	15.2	53	0.09	DTU [27]

Table 2. Overview table of the **CZTSe**-based cell efficiencies focusing on the absorber layers grown by different physical routes. Substrate temperature T_S, annealing temperature T_A, annealing atmosphere (Atm.), post-deposition annealing (PDA), anti-reflective coating (AR), bandgap energy E_g [eV], efficiency η [%], open-circuit voltage V_{OC} [mV], short-circuit current density J_{SC} [mA cm^{-2}], fill factor FF [%], area A [cm^2].

Route (Year)	T_S [°C]	T_A [°C]	Atm.	Notes	Buffer Type	PDA	AR	E_g [eV]	η [%]	V_{OC} [mV]	J_{SC} [mA cm^{-2}]	FF [%]	A [cm^2]	Institution References
Co-Evap. (2011)	330	560	S, Sn	**CZTSSe**: Cu, Zn, Sn, Se	CdS	No	/	~1.2	**5.4**	497	20	/	/	UL [28]
Co-Evap. (2012)	500	/	/	**CZTSe**: Cu, Zn, Sn, Se (7 Å s^{-1}), NaF layer	CdS	No	MgF_2	0.96	**9.1** (EA)	377	37.4	64.9	0.419	NREL [29]
Co-Evap. (2014)	450–490	/	/	**CZTSe**: Cu, Sn, Zn, Se (cracker)	CdS	No	No	~0.9	**7.1**	324	35.8	61	/	UL [30]
Seq. Evap. (2013)	/	/	Se	**CZTSe**: Submodule	CdS	/	Yes	/	**11.0**	516	34.1	62.5	14	Solar Frontier [8]
Co-Evap. (2015)	150	590	Se,N_2	**CZTSe**:Cu, Sn, Zn, Se (cracker), NaF	CdS	No	MgF_2	1.00	**11.6**	423	40.6	67.3	0.43	IBM [2]
Co-Evap. (2016)	200	525	$GeSe_2$, $SnSe_2$, Se	**CZTGSe**:Cu,Zn, Sn, Ge, Se	CdS	No	Yes	1.11	**12.3**	527	32.2	72.7	1.47	AIST [3]
Seq.Sputt. (2016)	RT	300–510	SeS_2, Se	**CZTSSe**:Cu/Sn/Zn/Mo, SeS_2/Se = 0.38%	CdS	No	No	1.097	**12.3**	521	34.98	67.2	0.185	DGIST [4]
Co-Sputt. (2017)	RT	560	Se	**CZSSe**:CuS, SnS, ZnS	CdS	Yes	No	~1.05	**9.7**	446	37.2	67	0.1	Uppsala [31]
Co-Evap. (2018)	275	550	S	**CZSSe**:Cu, ZnSe, Sn, Se (no grid)	CdS	No	No	1.17	**6.4**	422	25.9	58.2	0.09	UAM [32]
Monograin (2018)	/	740	/	**$CZTS_{3.2}Se_{0.8}$**:Cu, ZnS, ZnSe, Sn, S in KI	CdS	No	No	1.41	**12.0** (EA)	653	26.31	69.1	0.034	Crystalsol [33]
Seq.Sputt. (2018)	RT	400–550	Sn, Se,Ar	**CZTGSe**:Cu/Zn/ Sn/Cu/Mo, 12.5 nm-Ge	CdS	On cell	MgF_2	1.05	**11.8**	463	38.3	66.3	0.522	IREC [6]
Seq.Sputt. (2018)	RT	300–480	H_2S,Se	**CZTSSe**:Sn/Cu/Zn/Mo	CdS	No	MgF_2	1.13	**12.6**	541	35.39	65.9	0.480	DGIST [7]
Seq.Sputt. (2018)	RT	530	Sn, Se, N_2	**CZTSe**:Zn/CuSn/ Zn/Mo	CdS	No	No	1.03	**11.4**	443	38.1	68	0.36	UniOL [9]
Seq.Sputt. (2018)	RT	460–500	H_2Se,N_2	**CZGSe**:Cu/ Zn/ 200 nm-Ge/Mo	CdS	No	No	1.36	**7.6**	558	22.8	59	0.5	IMEC [34, 35]
Seq.Sputt. (2018)	RT	530	Sn, Se, N_2	**CZTSe**:Zn/CuSn/Zn, P_A = 10 mbar	CdS	No	No	/	**10.7**	433	38.8	64	0.33	UniOL [36]
Sputt.Quat. (2018)	RT	560	Ar, H_2Se	**CZTSSe**:Cu:Zn:Sn:S, Cd alloying	CdS	No	No	0.95	**11.2** (EA)	430	39.2	66.8	0.65	Tsinghua University [37]
Co-Evap. (2019)	340	550	SnSe, Se	**CZTSe**:Surface treatment, NaF	CdS	No	MgF_2	1.0	**11.7**	423	41.7	66.6	0.522	AIST [38]

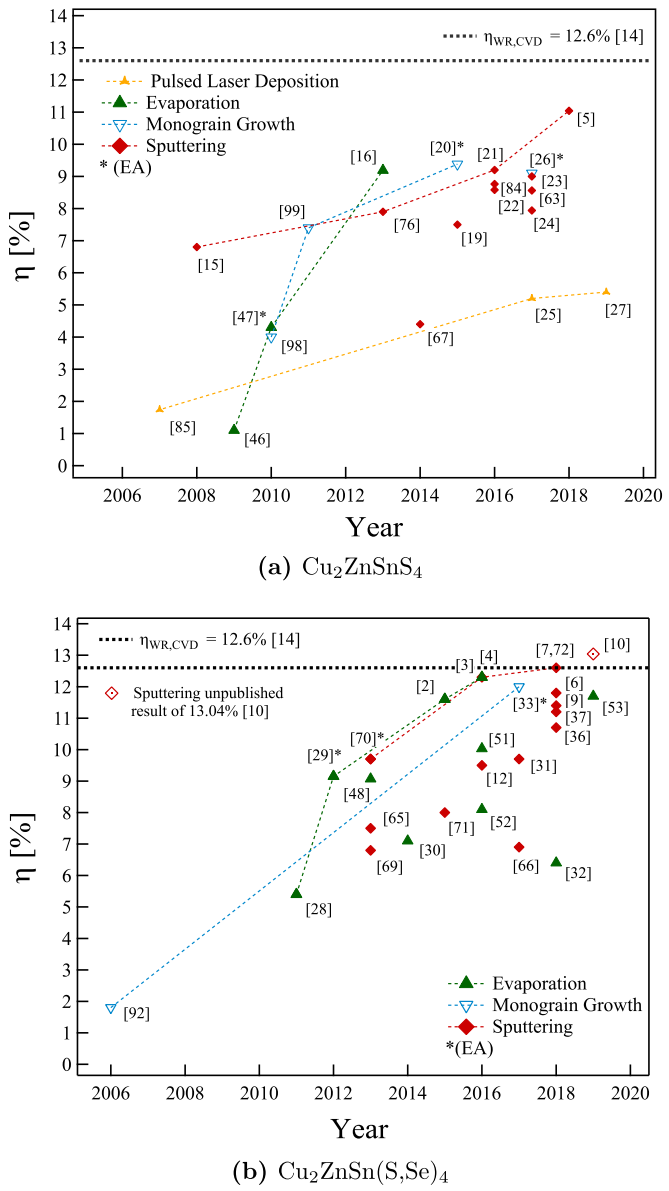

Figure 1. Evolution of the maximum efficiency η_{max} [%] for (a) CZTS-based and (b) CZT(S,Se)-based cells over the period of 2006–2019. In figure legend WR stands for world record and EA stands for effective area.

temperature T_A [°C] and atmosphere during post-deposition treatment (selenization and sulfurization), when available. These three parameters appear as the most relevant parameters concerning the thin film growth. Nevertheless, in order to provide the reader with a complete overview, the buffer type, the possible additional thermal treatment (post-deposition annealing (PDA)), the optional AR coating and relevant experimental information are presented in term of extra notes for each device.

The evolution of the efficiency over the last years is summarized for each physical route using two graphical representations: one for sulfide quaternary compound CZTS-based cells, (see figure 1(a)) and another one for selenide quaternary compounds CZTSe-based cells (see figure 1(b)). As a guide for the eye, a line is drawn between the maximum efficiency data points. Interestingly, even if the record efficiency for kesterite has been achieved using chemical routes and remained unchanged from 2012 [14], all the physical routes have experienced impressive progresses, showing sustained improvements over the last years. Concerning chemical vapor deposition aspects, those ones are addressed in another contribution of this journal issue.

2.1. One-step processes

One-step processes are based on co-evaporation of single elements onto pre-heated substrates. This approach has the advantage that in a single step the absorber is synthesized and crystallized.

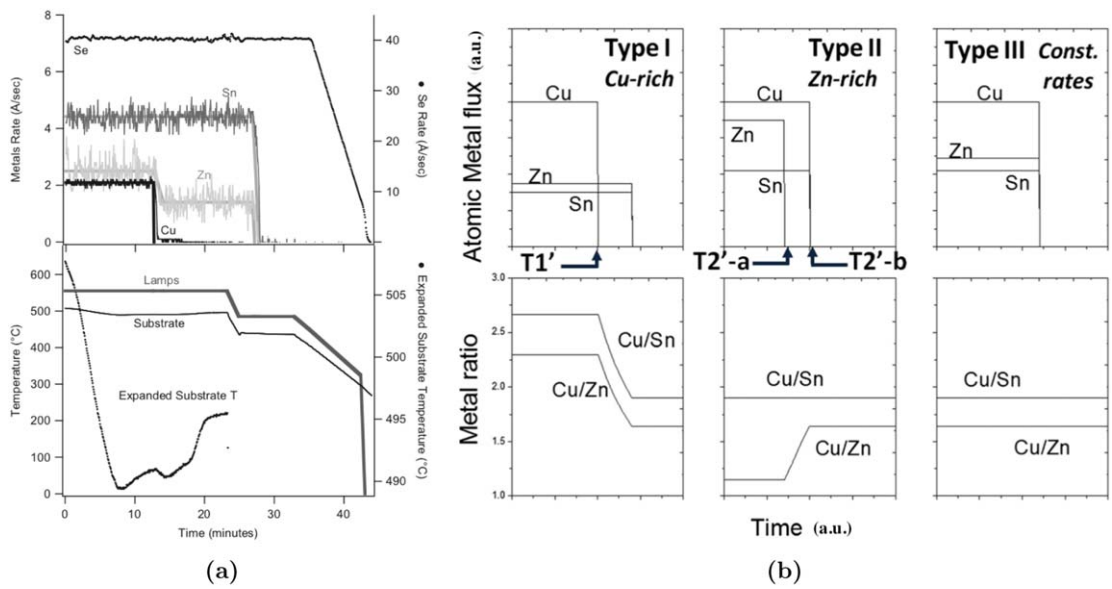

Figure 2. (a) Deposition data of the process for co-evaporated CZTSe materials reported by Repins *et al* [29]. Reprinted from [29], Copyright (2012), with permission from Elsevier. (b) Different composition regimes for co-evaporated CZTSe including Cu-rich, Zn-rich and constant rates by Hsu *et al* [48]. Reproduced with permission from [48] John Wiley & Sons. (Copyright © 2013 John Wiley & Sons, Ltd.).

Historically, co-evaporation of elements has been used for several years, resulting in the production of high efficiency $Cu(In,Ga)Se_2$ (CIGSe) thin film solar cells [39, 40]. In 1994, a three-stage process was developed, which is now regarded as a benchmark for the fabrication of CIGSe devices [41]. From CIGSe, it is well known that the ability to grow solar cell absorber layers in multiple stages, allowing the fluxes of each element and the substrate temperature to be varied simultaneously, offers a very effective way to introduce bandgap gradient, which reduces non-radiative recombinations at the interfaces and, consequently, leads to higher efficiency devices [42]. Laser light scattering, which had been developed to measure the stoichiometric point (Cu/(In + Ga) = 1) via optical methods [43] and pyrometry for *in situ* process control during a multi-stage co-evaporation process, provide endpoint detection signals for the transitions from Cu-rich to Cu-poor, which allowed the community to better understand the growth kinetics of the material and improve its properties [44, 45]. Currently the laboratory records for η are beyond 22%, while co-evaporated CIGSe on flexible foils have reached efficiencies above 20% and module efficiencies above 17% [7].

Despite the advantages and the knowledge gained from CIG(S,Se), co-evaporation of CZT(S,Se) has been revealed as very challenging from the beginning. In 2009, Cu_2ZnSnS_4 deposited by a high-temperature co-evaporation process without further annealing step led to the achievement of an efficiency of 1.1% [46]. In 2010, Schubert *et al* (HZB) synthesized CZTS absorber layers using a fast co-evaporation process [47]. The ~1.4 μm absorber layer was deposited in 16 min on a Mo-coated SLG substrate using ZnS, Sn, Cu and S sources. The co-evaporation process was performed at a nominal substrate temperature of 550 °C and at a sulfur partial pressure of (2–3) $\times$ 10^{-8} bar. Sulfur was evaporated using a cracker source with the effusion cell heated at 210 °C and the cracker zone heated at 500 °C. Using scanning electron microscope imaging (SEM), no apparent secondary phase was observed and energy-dispersive x-ray spectroscopy analysis showed a Cu rich and Zn poor composition. However a CuS secondary phase was observed using grazing incidence x-ray diffraction (XRD) and consequently removed by KCN etching. The finalized cell achieved an efficiency of 4.1% (effective area efficiency 4.3%) for $E_g = 1.51$ eV with $V_{OC} = 541$ mV, $J_{SC} = 13.0$ mA cm^{-2}, and $FF = 59.8\%$. The external quantum efficiency measurement also showed a substantial band tailing due to a large amount of lattice disorder.

These pioneering works demonstrated that, from the chemical equilibrium point of view, the loss of Sn-(S, Se) volatile species could be one of the major challenges to be overcome. In this sense, Repins *et al* reported a large improvement of co-evaporated CZTSe-based solar cells with an efficiency of 9.15% (EA) ($V_{OC} = 377$ mV, $J_{SC} = 37.4$ mA cm^{-2} and $FF = 64.9\%$) using a high temperature deposition ($T_S \sim 500$ °C) under a high Se background pressure, resulting in a Se deposition rate of 7 Å s^{-1} [29]. As shown in figure 2(a), the authors also used also a continuous Sn high evaporation rate in order to ensure effective incorporation and minimize the risk

of Sn-loss. In particular, Cu flux is stopped first to ensure Cu-poor conditions; Zn is then reduced but extended in time in order to ensure Zn-rich conditions.

In a subsequent work, Hsu *et al* [48] studied the impact of the deposition regime with Cu-rich, Zn-rich and constant rates (see figure 2(b)). They found that the complexity of the reaction process is due to the subtle reaction obstacle between CuSe and ZnSe species associated to the volatile nature of SnSe phases and/or the physical separation between the binary precursors. Additionally, they found no significant difference between Cu-rich and Zn-rich regimes in terms of morphology and conversion efficiency of the devices, suggesting that in the case of kesterites, CuSe phases act as crystallization flux in both conditions. The key challenge then remains the control of Sn-volatile species to provide an optimized route for the complete synthesis of the material.

On the other hand, in 2014, an efficiency of 7.1% ($V_{OC} = 324$ mV, $J_{SC} = 35.8$ mA cm^{-2} and $FF = 61\%$) was achieved by Redinger *et al* by synthetizing the absorber layer at a substrate temperature of $T_S \sim 500$ °C using both high deposition rates for Sn and SnSe compounds (respectively ~8 Å s^{-1} and ~3 Å s^{-1}) [30]. However, the authors observed that both methods still suffered from Sn losses. Even if the Se cracker allows to fine-tune the amount of Se flux and therefore the Se vapor pressure (which in turn contributes to the efficiency improvement), the maximum allowed (S,Se), Sn(S,Se) source(s) temperatures are limited at different values depending on the design of the machine. This constraint determines the ultimate substrate temperature, which can be used for the fabrication of the absorber layers. In the case of high temperature co-evaporation, the highest temperature is in the range of approximately 500 °C. Although this temperature is high enough to form quality kesterite absorber layers, the diffusivity of some elements is limited and consequently secondary phases are formed easily. The most prominent one is ZnSe [49], which forms especially at the early stages of the growth and which is quite difficult to remove at a later stage.

In view of all these progresses, the most important obstacle for high-efficiency solar cells using one step co-evaporation approach is probably the volatility of Sn-(S,Se) species. This has limited in large extent the further development of these methodologies, requiring the inclusion of an additional step at high temperature and under chalcogen and Sn atmosphere, which normally helps to correct possible stoichiometric deviations, and improves the growth of crystal grains.

2.2. Two-step processes

Two-step processes are the most widely used for the growth of kesterite absorbers. These experimental procedures consist in (i) a first deposition of a precursor film containing all (or part of) the chemical elements necessary for the kesterite phase formation, followed by (ii) a thermal annealing treatment under S (sulfurization) or Se (selenization) containing atmosphere, necessary to convert the precursor in a kesterite film and to promote the grain growth.

Different PVD routes can be used to deposit the precursor film, such as evaporation, sputtering and PLD methods. An overview of the most relevant results obtained by these three techniques is presented in the following sections.

2.2.1. Sequential evaporation/co-evaporation

As mentioned previously, even if evaporation/co-evaporation processes are regularly used for other chalcogenides to produce PV-grade material, the high volatility of Sn(S,Se) species normally induces to the formation of secondary phases during the growth process if high substrate temperatures are used. To minimize this risk, kesterite thin films have been deposited by co-evaporation at low temperature followed by annealing at higher temperatures in a specific atmosphere. In 2011, Redinger *et al* achieved an efficiency of 5.4% ($V_{OC} = 497$ mV, $J_{SC} = 20$ mA cm^{-2}) using co-evaporation of Cu, Zn, Sn and Se at a substrate temperature of 300 °C followed by an annealing in a graphite box in an excess sulfur atmosphere at 560 °C during 120 min [28]. They demonstrated that an annealing step at high temperature under Sn-containing atmosphere is highly necessary to compensate the Sn loss, and largely improves the properties of the co-evaporated layers. Much later, de la Cueva *et al* achieved CZTSSe-based devices with a performance of 6.4% ($V_{OC} = 422$ mV, $J_{SC} = 25.9$ mA cm^{-2}) using co-evaporation of Cu, ZnSe, Sn and Se at a substrate temperature of 275 °C followed by a subsequent annealing in a graphite box with sulfur excess at 550 °C for 60 min in Ar atmosphere [32].

Highest efficiencies for CZTS cells reported up to this date have been deposited via a process first reported by Shin *et al* in 2013 using co-evaporation of the elements at low substrate temperature ($T_S = 150$ °C), followed by a fast annealing at high temperature under N_2 atmosphere reaching an efficiency value of 8.4% [16]. The authors used a very thin CZTS absorber layer (~600 nm), estimating that this thickness is close to the estimated depletion width (~180 nm) summed up to the minority carrier diffusion length (>350 nm). This suggested that for the CZTS layers, very thin films are preferred, being an advantage for co-evaporation techniques that can easily produce such layers.

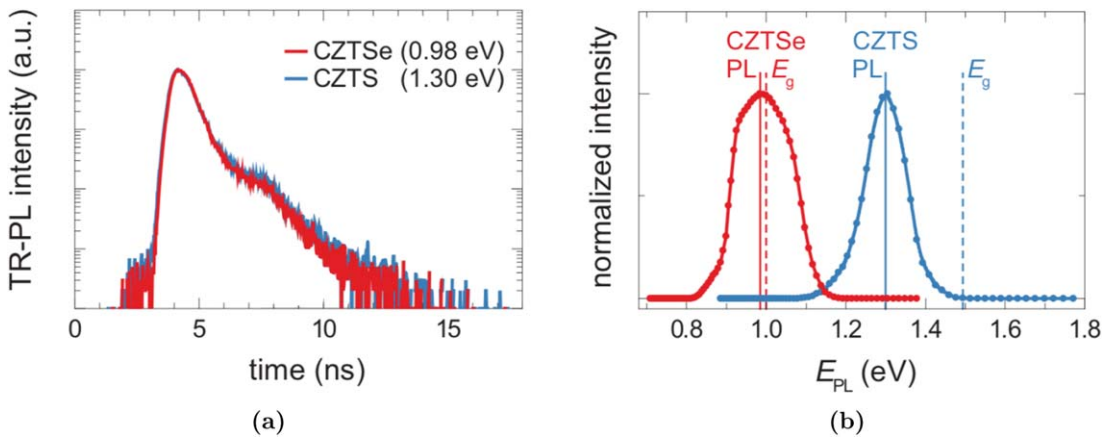

Figure 3. (a) Comparison of the PL decay obtained for both materials and, (b) comparison between PL main emission and E_g for CZTSe and CZTS. Reproduced with permission from [2] John Wiley & Sons. (© 2014 WILEY-VCH Verlag GmbH & Co. KGaA, Weinheim).

Aside from these developments, the pure Se-compound (CZTSe) typically provides better electrical properties as absorber layer than the pure S-compound (CZTS) (see figure 1(b)). The highest CZTSe-based cell efficiency has been reported by Lee *et al* in 2015 with $\eta = 11.6\%$ [2]. They also used a low temperature co-evaporation followed by a fast-thermal annealing under Se atmosphere at 590 °C. They found similar carrier lifetimes as for pure S-compound (see figure 3(a)), but with a smaller shift between the photoluminescence (PL) maximum emission peak and the bandgap (see figure 3(b)), suggesting that the reduction of the sub-bandgap states could be one of the explanations for the better efficiency of the pure Se-compound cell.

After these works, ever since 2013, various institutes such as NREL, IBM, AIST, University of Luxembourg (UL) and KAIST have focused mainly on the synthesis of pure selenide CZTSe, improving the efficiency of thermally-evaporated compounds [50–54].

For example, in KAIST, CZTSe thin films are deposited by thermal co-evaporation of elemental sources of Cu, Zn, Sn and Se. For the evaporation of Se, a thermal cracker is used. The substrate temperature during thermal co-evaporation of CZTSe is set at 150 °C. After the deposition of each elemental source, an additional Se layer of a few μm is deposited on top of the film, which provides Se-rich ambient conditions during PDA at 550 °C in a closed environment. The partial pressure of Se during the PDA is estimated to be around 40 mbar. Using this method the research team at KAIST has introduced passivated layers based on Al_2O_3 contact points at the back side using nanosphere lithography, and atomic layer deposition (ALD) of an Al_2O_3 layer at the front side. They demonstrated that both passivations can be relevant for the co-evaporation technology in particular, and for kesterites in general [53].

On the other hand, in comparison to chemical processes, the synthesis of kesterite absorber layers using co-evaporation provides a better reproducibility, higher material quality and safer methods to work with Se and/or S-compounds. The highest chemically synthesized cell efficiency has been achieved by Wang *et al* in 2013 using extremely toxic and reactive hydrazine solution [14]; therefore, considering the environmental concerns with the scale-up perspective, thermal co-evaporation has advantages compared to chemical routes. Also it is beneficial in terms of high throughput. Using this technique, it is possible to deposit uniform kesterite thin films whose composition differs by less than 5%–10% not only within a film but from film to film as well. However, the use of S and Se is detrimental for vacuum pumps such as cryo-pumps. Special maintenance on a regular basis is thus required.

2.2.2. Sequential sputtering/co-sputtering

Over the years, sputtering-based techniques have proved to be an efficient physical route for the synthesis of high efficiency thin film devices. This has been demonstrated both for chalcopyrite-based, as well as for kesterite-based solar cells [7, 10]. CZT(S,Se) growth processes based on the sputtering technique can be classified depending on the target(s) type(s) and on the deposition sequence. Either pure metallic (Cu, Zn, Sn), metallic alloys (Cu–Sn, Zn–Sn) [55–59] or chalcogen-containing (binary chalcogenides ZnS(e), SnS(e), $SnS(e)_2$ or $Cu_xS(e)$) [5, 60–62] targets and their combinations [36] have been used for the synthesis of kesterites as absorber layers. Concerning the deposition sequence, processes based on sequential [5, 6, 9, 56] or co-sputtering of different targets [61, 62], leading respectively to stacked-layer or homogeneously-mixed precursors, have been extensively investigated.

Co-deposition processes allow a faster deposition and a more homogeneous distribution of the elements in the starting precursor, thus allowing a faster reaction among elements, promoting the formation of the Cu_2SnX_3 ternary phase as intermediate reaction compound and minimizing (in principle) CZT(S,Se) decomposition and element loss.

Besides the progresses related to improvements in solar cell technology such as optimization of new buffer [23] and passivation layers [63], the efficiency progress is also due to the elucidation and improved control of the reaction pathways during the absorber formation. It has been shown that a route involving Cu_2SnX_3 (X = S or Se) and ZnX is preferred over reaction paths involving binary compounds (Cu_2X, SnX_2 and ZnX) [64, 36], since loss of SnS(Se) volatile species during the annealing treatment can be suppressed.

On the other hand, sequential sputtering allows modifying the stack structure to study and optimize the reaction pathway for kesterite formation. Moreover, by simply tuning the thicknesses and the stacked layers, control of composition can be easier when compared to co-sputtering route, which in contrast can suffer from cross contamination of the targets, when they are used simultaneously.

Both sequential and co-sputtering strategies have been successfully used to grow high quality CZTS and CZTSSe absorbers, leading to a continuous improvement of the device efficiencies. It is worth emphasizing, that current efficiency records for both CZTS (11.01% [5]) and CZTSSe (12.6% [7] or 13.04% from DGIST, KIER certified efficiency [10]) solar cells were obtained by using sputtering methods and there are several groups in the world with several examples of reported conversion efficiencies above 10% using these methodologies [5–7, 9, 65].

Some experiments based on sputtering from a single quaternary target (Cu_2ZnSnS_4 and $Cu_2ZnSnSe_4$) have been also reported in the literature with successful results [37, 66, 67]. An historical review of the main progresses obtained with different sputtering methods is presented here below.

Sequential sputtering

First approaches using sequential sputtering for kesterite were reported by Shimada *et al*, who compared metallic stacks and chalcogen containing stacks [68]. The progresses in these routes showed that the use of metallic stacks provides for the moment better efficiencies at least for the selenide compounds, with University of Oldenburg (EHF/LCP group) reporting 11.4% [9], IREC 11.8% [6] and DGIST a 12.6% efficiency device [7]. Furthermore, a certified efficiency of 13.04% has been obtained using sputtered precursors [10], whereas for pure sulfide kesterite compounds the best results are instead obtained using S-containing targets [19] and/or co-sputtering approach.

Using the sequential sputtering route, different strategies have been adopted by different groups to control the reaction mechanisms in order to minimize or avoid the loss of volatile constituents such as metallic Zn and Sn(S,Se) [6, 36] and the uncontrolled formation of secondary phases.

The use of a mixed Cu–Sn target was proven to reduce the Sn loss by driving the system towards the formation of related ternary compounds Cu_2SnX_3 (with X = S or Se), rather than binary volatile SnX phases [36] during the annealing treatment. This strategy was adopted by the EHF/LCP group from the University of Oldenburg, which recently reported a CZTSe-based device with efficiency of 11.4% [9]. The absorber was grown from a Zn/CuSn/Zn stacked elemental and alloy precursors annealed under excess Se atmosphere with added elemental Sn in a quasi-closed graphite box in a conventional closed tubular furnace (530 °C for 20 min). The reactor pressure (adjusted with N_2 inert gas) was shown to play a crucial role for the final stoichiometry by drastically affecting the Zn and Sn content in the final film. In particular, it was shown that an annealing pressure around 10 mbar allows the minimization of loss of volatile species, with very small stoichiometry fluctuations observed between 5 and 20 mbar. This was described as an equilibrium-like behavior of the system in this region, with spontaneous compensation of potentially lost species. The latest developments of the process include a growth of Cu-poor CZTSe via an intermediate Cu-rich state, which appears to further stabilize the reaction path and allows for more defined control of the final material properties. It is worth mentioning that no chemical etching is employed to clean the absorber surface before solar cell production and that the selenization is performed by a facile one-step process.

A different approach to improve the control of absorber composition is based on the optimization of the metallic precursor stack structure to avoid element loss [69, 70]. Different stack sequences have been investigated by the research group at IMEC [69, 70], reporting a maximum efficiency of 7.5% using elemental metallic stacks with the structure Cu/Zn/Sn/Mo [65] and 9.7% (EA) (exceeding 10% for smaller lab cell areas) by replacing the Sn target with a mixed $Cu_{10}Sn_{90}$ alloy (Cu/Zn/CuSn/Mo precursor) [70]. A different stack order was adopted by the research group at IREC, where precursors are deposited on a specially designed Mo tri-layer [12] with the typical structure Zn(165 nm)/Cu(175 nm)/Sn(275 nm)/Cu(5 nm)/Mo, used to obtain Cu-poor (Cu/(Zn + Sn) = 0.72) and Zn-rich (Zn/Sn = 1.05) compositional ratios. Several reasons lead to this specific stack order. First, a 5 nm thick Cu layer is deposited in order to improve the wettability of Sn onto the Mo substrate and also to improve the homogeneity of this layer. Then a 275 nm layer of Sn is deposited at the back of the absorber layer to delay and avoid evaporation of Sn(S,Se) phases as much as possible. Subsequently, 175 nm of Cu are

additionally grown in the middle to allow for easier formation of alloys with Sn (bronzes) and Zn (brasses) which consequently stabilize both species. Finally, a 165 nm thick Zn layer is deposited in excess at the top of the absorber layer in order to keep the excess at the surface for further removal.

The metallic stack is then submitted to a reactive annealing under Se and Sn atmosphere using a graphite box in a tubular furnace, with a first annealing step at 400 °C for synthesizing the kesterite and a second step at 550 °C for its improved crystallization. This process allows to reach a baseline efficiency of about 8.5%. Then, a great efficiency improvement has been recently obtained by doping the absorber with a few nm of Ge: a device with efficiency of 11.8% has indeed been reported in [6]. Besides the beneficial effect on the grain growth (see section 2.4.1)∗, Ge is also found to induce fundamental changes in the formation mechanism of the kesterite absorber, promoting a stabilizing Cu–Sn intermixing, resulting in the suppression of Sn-loss [6].

A device with an efficiency of 12.6% [7] was fabricated by DGIST group using a mixed sulfide-selenide kesterite absorber obtained from an elemental metallic precursor stack (Sn/Cu/Zn/Mo), converted into a CZTSSe film by a sulfo-selenization treatment. Several process improvements regarding the optimization of both the precursor structure and the annealing treatment allowed us to reach this successful result. A CZTSSe device with efficiency beyond 8% was initially obtained in 2015 by the selenization at 570 °C of a chalcogen containing precursor Cu/SnS/ZnS/Mo [71]. A great improvement (12.3%) was then obtained by replacing the base Cu/SnS/ZnS/Mo precursor with a Cu(170 nm)/Sn(268 nm)/Zn(188 nm)/Mo pure metallic stack [4] and developing a sulfo-selenization process at 510 °C using SeS_2 and Se as chalcogen sources. Due to the stepwise release of chalcogen elements from the SeS_2 source, the incorporation of S and Se throughout the absorber changes during the heating and the cooling process, resulting in an optimized bandgap graded CZTSSe absorber. An additional improvement (12.6%) was finally obtained by further optimizing the precursor stack (Sn (275 nm)/Cu(160 nm)/Zn(190 nm)/Mo) and the annealing treatment, performed at 480 °C at slightly below 1 bar using H_2S and Se as chalcogen sources. Using this specific process, the authors reported first the rearrangement of Cu, Zn, and Sn metal compounds and secondly the reaction at low temperatures of most Zn with S and Se to form a ZnSSe shell leading to the formation of voids. Since voids and secondary phases mainly exist near the back contact, the top of the CZTSSe absorber layers showed a large-grained and phase-pure structure leading to efficiency results over 12% [72].

In addition, DGIST achieved an efficiency of 13.04% certified by KIER (Korea Institute of Energy Research) [10]. At the time of the writing, the detailed characterization result of the above-mentioned high efficiency devices has not been published yet.

Co-sputtering

The first report of the co-sputtering route as a possible effective way to produce high efficiency kesterite-based devices was published in 2008 by Katagiri group [15], producing a CZTS solar cell with an efficiency of 6.8% via sulfurization of a co-sputtered precursor from three targets (Cu, ZnS and SnS). Thereafter, extensive research in this route led to a great efficiency improvement, especially for pure-sulfide compounds which recently reached a new world-record efficiency of 11.04% [5]. In the case of mixed CZTSSe-devices obtained by a co-sputtering method [73–75], the best efficiency is 9.7% [31], well below the efficiencies reached with sequential sputtering approach, whereas no pure selenide device grown by co-sputtering route has been reported so far. For this reason, this section will be mainly focused on progresses related to CZTS based devices. Sputtering routes based on the deposition from a single quaternary target will be also described here, being often classified as a special case of co-sputtering methods.

Different co-sputtering approaches have been reported in the CZTS literature over the years. First, experiments based on reactive co-sputtering of metallic targets (CuSn and ZnS) in Ar/H_2S atmosphere were reported by the group at Uppsala University, with a remarkable efficiency of 7.9% reached in 2013 [76]. This approach allows for a homogeneous precursor with a tunable composition and a stoichiometric amount of sulfur, which can be rapidly annealed to obtain large grains. However, the challenging control of the long-term process stability (due to a change of the state of the targets, of the deposition rates and of the precursor composition) made this reactive route less appealing compared to simplified non-reactive sputtering methods [77].

Nowadays, the most widely and successfully used co-sputtering processes are based on (i) binary compound or (ii) mixed metallic—compound targets, sputtered in an inert atmosphere. The main difference between these two approaches is the chalcogen amount in the starting precursor, which is close to the stoichiometric amount in case of CuS, SnS and ZnS targets and it is lower when one or more binary compounds are replaced by the pure elemental targets. Both approaches were proven to give successful results, with a recent efficiency record of 11.04% [5] and many groups reporting devices with efficiency close or higher than 8% [22–24].

The progresses with the co-sputtering route are mainly due to the advances in the annealing step, whose process conditions strongly influence the properties of the final absorbers and respective devices.

However, it is worth observing that the efficiency progresses are not only related to the improvement of the growth process, but are very often associated to other advancements in the solar cell technology, such as the optimization of back-side passivation layers and, most importantly, of new buffer layers alternative to CdS [21, 23, 78]. This latter point is particularly important for CZTS devices because of the well-known not-optimum band alignment between CZTS and CdS [79, 80]. Moreover, PDA treatments, performed either on the bare absorber [81] or on the CZTS/CdS samples [5] or even on complete devices [24] have been also proven to boost efficiencies. All these points must be taken into account when device performances are compared since, often in this framework, the efficiency is not a measure of the quality of the growth process alone.

Concerning the progresses in the annealing step, an important efficiency improvement was first achieved in 2016 by the Shenzhen Institutes of Advanced Technology [22], reporting a CZTS device with an efficiency of 8.58% obtained after the optimization of the heat treatment, in order to minimize the Sn loss. The absorber was grown on Mo-coated SLG by co-sputtering of SnS_2, ZnS, and Cu targets, followed by a two-stage sulfurization process: the first annealing step was performed at low temperature (260 °C) in N_2 (95%)/ H_2S (5%) atmosphere (0.4 bar) for 75 min to form a CZTS phase, minimizing the decomposition of SnS_2 into volatile SnS and S_2; the second step is performed in the same atmosphere at higher temperature (510 °C for 15 min) to eliminate secondary phases and to increase the grains dimensions. According to the authors, the device obtained using this two-step thermal treatment exhibited a higher hole concentration, lower defect density and a shallower trapping energy than the device formed by a conventional single-step slow ramping annealing process.

In 2017 an additional advance in CZTS device efficiency was reported by the group at Uppsala University [23]. In this case, the CZTS absorber was grown by co-sputtering of CuS, SnS and ZnS binary sulfide targets and was then sulfurized in a graphite box with additional S-powder, inside a tube furnace under a static N_2 pressure of 350 Torr for 13 min at 580 °C. For room-temperature sputtering, cracking or peeling of precursors was observed after annealing [82], while improved adhesion was seen for temperatures around 150 °C–250 °C. The final CZTS films were etched for 2 min in 5 wt% KCN, rinsed in deionized water just before the CdS buffer layer deposition. The best efficiency reported using the standard CdS buffer layer was 7.2%. However, a better device with efficiency 9% was obtained by replacing CdS with an optimized Cd-free ZTO buffer layer deposited by ALD. The ALD process temperature was set to 145 °C.

In the same year, a device with an efficiency 7.94% was produced by the ENEA group [24] using a Cu–SnS–ZnS co-sputtered precursor, annealed for 1 h in a mixed N_2–S atmosphere, under gas flow conditions, using a custom system with two independent chambers for the precursors (at about 570 °C; heating rate 20 °C min^{-1}) and for the sulfur source (at about 260 °C). The sputtering process was carried out without any intentional heating of the substrate and at a working pressure of 5×10^{-3} mbar, optimized to improve the adhesion of the final CZTS film on the substrate. It was shown that lower working pressures during precursor processing tend to increase the compressive stress in the films, then leading to blister formation during the later annealing treatment [83].

Compared to previous annealing experiments performed in a tubular furnace using a semi-closed chamber (not published), the optimized annealing system allows to produce devices with an improved CZTS/CdS junction quality (without any hazardous chemical etching, like those based on KCN), as demonstrated by reverse saturation current densities as low as a few nA cm^{-2} [24]. Even in this case, the efficiency progress cannot be simply ascribed to the optimization of the growth process, but also to a strong beneficial effect of PDA treatment performed on complete devices [24]. Physical mechanisms underlying the PDA effects are discussed in another paper of this journal issue.

Starting from similar Cu–SnS–ZnS co-sputtered precursors, further increased efficiencies have been reported between 2016 and 2018 by the UNSW group after several optimization steps of both annealing and device processings.

In 2016 an optimized annealing treatment performed at 560 °C for 5 min (heating rate 15 °C min^{-1}) in a combined S and SnS atmosphere allowed the improvement of the device efficiency from 6.16% (for S-only annealing atmosphere) and 7.52% (for S-only annealing atmosphere followed by PDA) to 8.76% [84]. The efficiency improvement was ascribed to an improved CZTS/CdS front interface, whose microstructure and chemistry strongly depend on the sulfurization conditions and post-annealing treatment. A detailed tunneling electron microscope analysis proved that the use of a mixed S-SnS atmosphere yields a CZTS absorber with a well-structured surface, enabling a quasi-epitaxial growth of the CdS buffer on CZTS (leading to free-lattice-defects interface) while promoting the Cd diffusion into the CZTS surface region (which is believed to facilitate a more effective buried homojunction). This results in longer carrier lifetime, higher V_{OC} and FF values compared to devices obtained by annealing the CZTS in S-only atmosphere.

Efficiencies of 10% and then 11% were then reported in 2018 by Yan *et al* [5], establishing the new world record device for only sulfur-based kesterite solar cells. Compared to their previous work, the annealing treatment was still performed in a combined S-SnS atmosphere, but the heating ramp was reduced to

10 °C min^{-1} and the cooling rate was controlled at 30 °C min^{-1} to avoid the formation of blisters. The sputtering rates were set to confine the Cu/Sn ratio within 1.7–1.8 and Zn/Sn $\sim$ 1.2.

Moreover, the CdS/CZTS heterojunction was treated with a PDA at 300 °C for 10 min under a N_2 atmosphere using a two-zone tube furnace. It is worth noting that, despite not clearly specified in the case of their record device, the significant efficiency improvement of the UNSW group could be also partially due to the use of a back side passivation layer of Al_2O_3 to improve the CZTS absorber stability, as previously reported by the same authors [63].

Sputtering from a single quaternary target

Besides the sequential and co-sputtering approaches, the use of sputtering processes based on a single CZTS compound target have also been reported in literature as a promising strategy for the production of kesterite absorbers since, similarly to sequential sputtering, only one power source is required, but with no need to control the thickness of the stack layers to adjust the composition.

A first comparison between CZTS-solar cells prepared by single sputtering of CZTS compound and co-sputtering of Cu, ZnS and SnS targets was reported in 2014 by the Katagiri group [67]. In both cases, the precursors were annealed at 500 °C in H_2S containing atmosphere. The final CZTS thin films exhibited similar properties in terms of the crystalline structure, the optical absorption and the chemical composition; however, compared to co-sputtering, the single sputtering process produced samples with a better morphology without any voids, leading to devices with higher efficiencies (4.40%). Despite these results, higher efficiencies for CZTS solar cells were then obtained by further optimizing the co-sputtering route.

The use of single target approach led to more successful results in the case of mixed CZTSSe absorbers, grown by selenization of CZTS quaternary precursors. In the work by Lin *et al* [66], a device with cell efficiency of 6.9% was obtained by optimizing the S/S + Se ratio using a sulfo-selenization treatment, varying the ratio of Se and S powder during the heat treatment at 570 °C. The optimum chalcogen ratio was found to be S/S + Se = 0.46, yielding the best transport properties (p-type carrier concentration of 2.17×10^{15} cm^{-3} and mobility of 8.9 cm^2 V^{-1} s^{-1}) and the best device performances.

More recently, Sun *et al* [37] reported efficiencies beyond 11% for CZTSSe solar cells (sulfur about 1%) by cadmium alloying. The absorber layer was grown from a CZTS precursor sputtered from a single compound target and selenized in H_2Se/Ar atmosphere after the deposition of a CdS layer (50 nm) on the top surface. XRD and Raman characterizations showed that Cd alloyed into CZTSSe lattice during the heat treatment (with a calculated Cd/(Cd + Zn) ratio of 0.13), enhancing the grain growth and improving the homogeneity of the Sn/Cu ratio along the thickness compared to the reference device (with efficiency 8.5% without Cd alloying), even if some small grains with increased Sn/Cu ratio are detected near the back contact. The improved performances of Cd-alloying CZTSSe devices were also attributed to the effect of cadmium on the bulk acceptor defects, showing shallower energy levels and slightly higher concentrations compared to the reference sample, thus resulting in a higher hole density, a lower Fermi level and a higher V_{OC}. A beneficial effect of Cd alloying on possible defect clusters and deep defects is also suggested, thus explaining the enhanced J_{SC} due to a weaker recombination loss. Moreover, Cd alloying samples showed a reduced interface recombination, not yet explained, but likely related to the higher Cd content detected near the absorber surface by secondary ion mass spectrometry.

2.2.3. Pulsed laser deposition

In 2007, Moriya *et al* produced the first CZTS thin films using PLD at Nagaoka University of Technology. This cell achieved a rather low efficiency of 1.74% [85]. In 2015, the first Cu_2SnS_3 (CTS) thin film was produced by PLD [86, 87]. Some achievements of both CZTS and CTS thin films growth can be found in review articles by Sulaiman *et al* [88] and Vanalakar *et al* [89]. Then, since 2015, DTU initiated a program on CZTS absorber layers grown by PLD. As presented in figure 1(a), solar cell efficiencies based on PLD-grown absorber layers continuously increased and the largest value of 5.4% has been reached recently [27].

A typical 0.4–1 μm thick CZTS thin film is deposited on a Mo-coated SLG substrate by PLD in a vacuum chamber of 10^{-6} mbar. A composite target with the overall stoichiometric composition Cu_2ZnSnS_4 or Cu_2ZnSnO_4 is struck by a KrF excimer laser beam. After the deposition, the films were annealed in a graphite box with a S overpressure at a temperature ranging from 550 °C to 600 °C. Using this two-step technique, a first efficiency record of 5.2% was obtained by Cazzaniga *et al* in 2017 [25] and subsequent cells were completed by Gansukh *et al* from DTU [27]. Using PLD, one important deposition parameter turns out to be the laser energy per unit area [J cm^{-2}] on the composite target. It has been observed that the stoichiometry of the deposited film depends strongly on this deposition parameter as described by Schou *et al* [90]. For the sulfide record cell (see table 1), the desirable stoichiometry with a Cu-poor and Zn-rich film could only be obtained for a fluence in the range of 0.7 to 1 J cm^{-2}. One observation concerning the reproduction of the target composition was that films fabricated with low fluence were extremely Cu-poor, while films produced at high fluence were Cu-rich. This was the case not only for films produced from composite targets, but also for single-phase CZTS targets. For oxide targets, CZTO, it was necessary to apply a target with less copper than the standard composition [25, 90].

This strong dependence on fluence and in a more technical way, the frequent cleaning of the vacuum windows account for issues concerning the synthesis of kesterite as absorber layer using PLD. Several advantages are also provided by this PLD technique. (i) The superthermal energy of the particles ($\geqslant$20 eV) improves the mobility on the surface which gives a high crystallinity and strengthen the adhesion to the underlying layers. This advantage is shared by energy-enhanced deposition technique like PLD and sputtering. (ii) PLD with oxide targets may also greatly ensure a homogeneous chemical composition in the deposited film [91]. However, several issues significantly hurdle the production of high-efficiency solar cells based on absorber layer grown by PLD:

1. At high laser fluence the fast ablated ions can induce sputtering of the growing film, which leads to a surplus of the species with the highest cohesive energy in the film [90].
2. Running the laser with a stable beam energy is also a complicating issue leading to difficult process reproducibility [25].
3. The main difficulty is the small number of samples which can be produced in each run. This makes PLD cumbersome, and it also means that a lot of runs are necessary for optimizing the sulfurization process.

Moreover, laser equipments are expensive and this may be the strongest obstacle for a wide-spread use of PLD in PVs.

2.3. Growth of monograins

During the last decade various quaternary compounds like $Cu_2ZnSnSe_4$, Cu_2ZnSnS_4, $Cu_2ZnGeSe_4$, Cu_2CdSnS_4, $Cu_2CdGeSe_4$ and their solid solutions have been synthesized by using monograin powder technology. As presented in figure 1(b), in 2006, the first kesterite based monograin layer (MGL) solar cell with the structure of ZnO/CdS/$Cu_2ZnSnSe_4$/graphite showed an efficiency of $\eta = 1.8\%$ with output parameters as follows: $V_{OC} = 401$ mV, $J_{SC} = 15.5$ mA cm^{-2}, $FF = 41\%$ [92]. In 2008, the first Raman spectra for kesterite materials was published by Altosaar *et al* [93] from Tallinn University of Technology (TalTech). In 2009, Grossberg *et al* [94] used PL measurements to clarify the correct bandgap energy for CZTSe and according to their experimental results, confirmed that the bandgap energy of CZTSe is 1.02 eV at $T = 10$ K. In addition, in [95–97] the solid solutions of $Cu_2ZnSn(Se_xS_{1-x})_4$ monograin powders were investigated for the first time by XRD, PL, Raman and x-ray photoelectron spectroscopy (XPS) measurements.

Over the years, improvements in solar cell efficiencies have been obtained due to the optimization of post-treatments of crystals surfaces by chemical etchings and annealing in chalcogenide-containing atmospheres. Currently, the highest efficiency of Cu_2ZnSnS_4 MGL solar cells is 9.38%, achieved by Kauk-Kuusik *et al* [20] (see table 1). Efficiencies of up to 9.5% of CZTSSe MGL devices with an approximate active area ratio of about 80% were certified. The conversion efficiency of the active CZTSSe material is in the range of 12% [33] (see table 2).

The most effective Cu_2ZnSnS_4 monograin powders have been synthesized under Cu-poor and Zn-rich conditions from high purity (5 N) elemental or binary precursors in molten KI as water-soluble flux material. The mixture of precursors and KI in the desired amounts and ratios are grounded in a ball mill, loaded into a quartz ampoule, degassed under dynamic vacuum and sealed. The sealed ampoule with the mixture of components is annealed at 740 °C. The temperature of synthesis should be above the melting point of the flux material (~681 °C) and lower than the melting point of kesterites (~990 °C). The processes of formation and growth of the semiconductor compound crystals take place in the liquid phase of the used flux material. The crystal size of the quaternary compound materials could be controlled by the temperature and the time of the growth as well as by the chemical nature of the flux used in the growth process. After cooling down and opening the ampoule, the salt is removed from solid powder particles by leaching with deionized H_2O. Finally, the released monograin powder is dried and sieved into several narrow granulometric fractions between 45 and 112 μm. Timmo *et al* from TalTech showed that the chemical etching of as-grown powder crystals is required for modifying of the surface composition of the absorber material crystals and finally improves the parameters of MGL solar cells [98]. The combined chemical etching of absorber materials with 1% Br_2 in methanol solution followed by 10% KCN solution results in the increase of the values of solar cell parameters due to the removal of the secondary phases from the crystals surfaces. Kauk-Kuusik *et al* reported that the efficiency of MGL solar cells improved remarkably if the chemically etched CZTS absorber crystals were additionally post-annealed in a sulfur-containing atmosphere [99]. The optimal heat treatment for the CZTS powder was done in a two-temperature zone tube furnace at 740 °C in sulfur atmosphere under a pressure of 1.3 bar. Further improvements in the performance of CZTS MGL solar cells (in particular the V_{OC} and FF parameters) were achieved by using oxidative chemical treatment before the buffer layer deposition process [20]. An XPS analysis confirmed the formation of SnO_x layer on the absorber surface after bromine-etching that acts as an interface

passivation layer and improves CZTS device performances [20]. This kind of combinational treatment results in the efficiency of 9.4% for CZTS MGL solar cells.

As the V_{OC}-deficit issue exists also in MGL solar cells, the influence of low-temperature structural ordering of the absorber material on the performance of Cu_2ZnSnS_4 MGL solar cells was investigated by Timmo *et al* [26]. An improved ordering in the crystal structure resulted in the highest V_{OC} value of 784 mV for CZTS MGL solar cell. However, the overall performance was decreased due to lower values of *FF* and J_{SC}. The optimal conditions for improving the efficiency of CZTS MGL solar cells from 8.1% to 9.1% by using the low temperature annealing process were found to consist in a 4 h long annealing at 150 °C after cooling from 740 °C to RT for 5 min. PL and *J*–*V* characteristics showed that changes in Cu–Zn ordering is accompanied with changes in the radiative recombination mechanism from band to tail to deep-trap related recombination in most ordered material, reducing the positive effect on the CZTS solar cell performance [26].

MGL technology combines advantages from two techniques:

1. The monocrystalline nature of the material.
2. The greater freedom in the choice of dimensions and electrical parameters of the thin film technology. However, compared to thin film technologies, MGL solar cells have a maximum working area of 80% of the total area due to the polymer binder between the crystals.

The main feature of MGL technology is that the fabrication of the absorber/junction formation and the cell/module formation is separated, which leads to several benefits in both stages of MGL solar cell production. The advantages of the developed powder materials are: (i) single-crystalline structure of every grain; (ii) uniform distribution of doping impurities; (iii) possibility of making flexible devices due to variability in size and form; (iv) minimum waste of material.

2.4. Discussion

In this section, key aspects related to the final properties of the different absorbers obtained using physical vapor deposition routes are discussed. In particular, we select three main aspects considered very relevant for these technologies, i.e. morphology, alkali doping and alloying (mainly for graded bandgap). In addition, a final section dedicated to kesterite-based submodules is presented.

2.4.1. Morphological properties

The use of physical vapor deposition methodologies can have a distinct impact on the morphology of the synthesized layers when compared with chemical-based ones. When optimizing synthesis processes of physical vapor deposition, film adhesion, formation of voids at the back contact and grain size are the main issues to consider. Considering the experience accumulated for other chalcogenides such as CIGSSe, the adhesion onto glass/Mo substrates is expected to be good, if one can control the formation of $Mo(S,Se)_2$ and the synthesis parameters. In fact, the uncontrolled sulfurization/selenization of Mo can have a strong impact on the adhesion properties of the absorber on the substrate [100].

An additional challenge inherent to the preparation of kesterite films is the formation of volatile species, which can lead to issues on the back contact region, namely lack of adhesion and formation of voids. Kim *et al* [101] improved the adhesion at the back region of the CZTS by introducing a thin Sn layer between the CZTS and the substrate. The improvement was attributed to the reduction of the ZnSe secondary phase. Using nanoindentation, Yin *et al* [102] demonstrated that S-containing kesterites exhibit better adhesion to the substrate than pure selenide kesterites, which is likely related to the different mechanical properties of both types of chalcogenides. Malerba *et al* investigated the blistering effect of CZTS films prepared by co-sputtering deposition of precursors followed by reactive annealing [83]. They observed that the likelihood of the blisters formation (see figure 4) is closely related to the background pressure during the sputtering process; it can be drastically reduced at increased pressures. Additionally, they developed a stress-driven model for viscoplastic deformation and concluded that gas entrapment only contributes as a secondary effect, contrary to the common intuition.

Another problem frequently encountered in kesterite synthesis is the presence of voids at the back region. This problem was observed for both sulfide or selenide compounds prepared by physical routes [103–105]. It is clear that the density of voids largely depends on the synthesis parameters including annealing conditions [106, 107] and the stacking order of the precursor layer in the case of sequential sputtering method [108]. The origin behind the formation of these voids is still not well understood but it is expected to be related to stress at the back region, the volatility of Sn-related species and the possible decomposition of kesterites in contact with Mo and/or fast Cu out-diffusion during the annealing. During the past several years some interesting technological solutions have been proposed to suppress the formation of voids at the back contact and most of

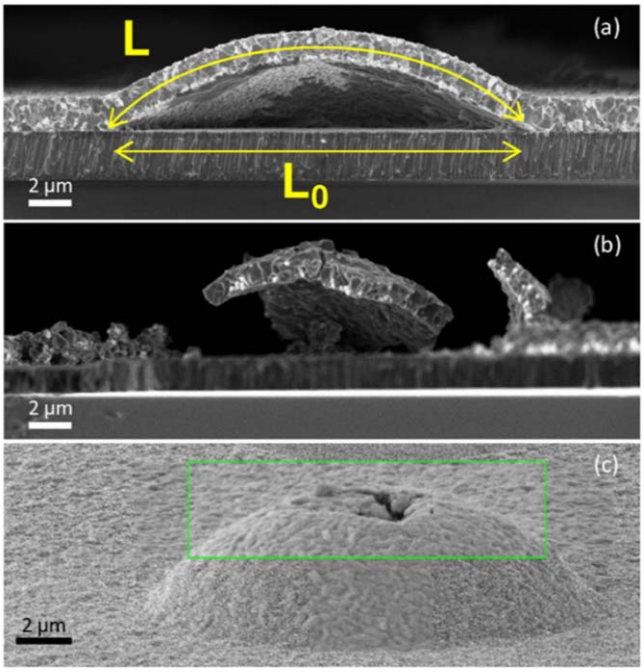

Figure 4. SEM observations of typical blisters showing the bending effect. Reproduced with permission from [83], Copyright (2016), with permission from Elsevier.

them rely on the use of an interlayer including oxides [109], nitrides [110] and different metals [111] and have shown improvements not only in the morphology, but also in the performances of the resulting solar cells. Recently, an interesting observation with regards to the back contact voids was reported; the detection of voids has been typically made from lamella samples prepared by focused ion beam (FIB) [105, 112, 113]. The authors claimed that the use of a FIB process was responsible for the void formation, not the film synthesis process itself, because the FIB process can preferably sputter Zn and ZnX (X = S or Se).

Finally, regarding the grain size, very large grains can be obtained with different physical vapor deposition techniques for various cationic (Ge,Cd) and anionic (S,Se) variations of kesterite compounds. Figure 5 compares kesterite absorbers obtained using different physical vapor deposition techniques in several institutions worldwide, demonstrating that obtaining large grain sizes can be easily accessible by controlling the synthesis and the PDA parameters.

2.4.2. Alkali doping

As kesterite materials are one derivative of the chalcopyrite $CuInSe_2$, many CIGS technologies could be introduced to CZTSSe-based materials and solar cells. One of the most important technologies for CIGS solar cell is alkali doping, which is indispensable for high efficiency CIGS solar cells. Various effects of alkali doping were reported in CIGS solar cells: enhancement of grain growth, increase of hole concentration, passivation of interface and grain boundaries, improvement of lifetime and of V_{OC} [115]. Recently, high conversion efficiencies in CIGS solar cells were obtained using heavier alkali doping, such as Rb and Cs doping [116, 117]. However, these effects have not been reported in kesterite solar cells.

Drastic morphological changes by Na doping have been reported in several papers. The morphology and the grain size of CZTSSe were systematically investigated by Sutter-Fella *et al* as a function of the deposited NaF layer thickness [118]. The grain size was found to increase with increasing the NaF thickness. The enhancement of grain growth was found to be due to the formation of a liquid Se–Na phase on the top of CZTSSe surface. Interestingly, although the grain size increased with NaF insertion, the PV properties did not correspond to the increase of grain size. The highest conversion efficiency was obtained with larger grains compared to that without NaF insertion. However, the grains for the best-performing cell were much smaller compared to the largest grains reported in the article. This implies that Na doping in kesterite works not only as the grain growth promotor but also promotes other functions, which is a similar feature in CIGS.

The conversion efficiency and especially the V_{OC} of CIGS solar cells are widely known to increase by alkali doping because of the improvement of minority carrier lifetime, and the increase of carrier concentration. However, the relationship is not straightforward in CZTS solar cells. It is reported that the lifetime of CZTS has a

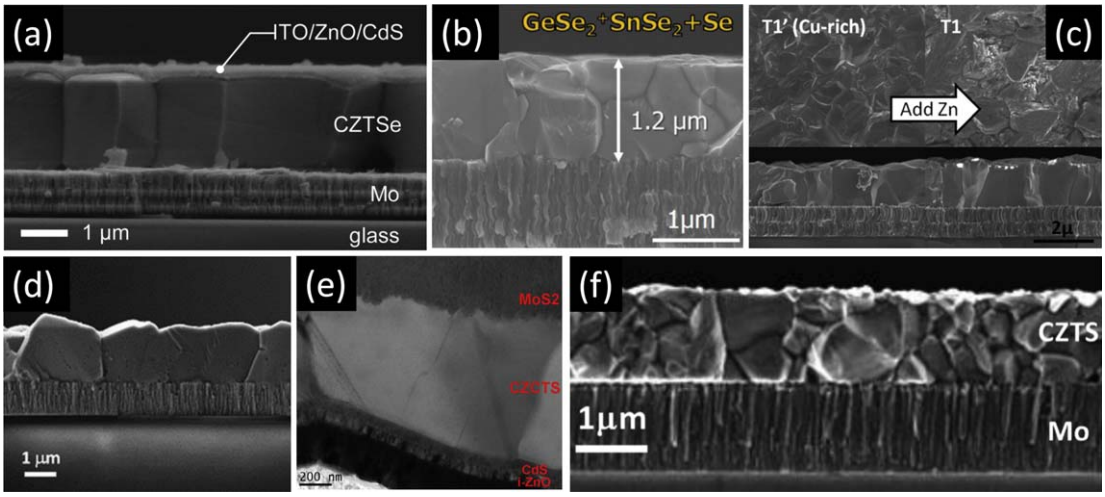

Figure 5. Cross sectional images of kesterite absorbers reported by different groups showing large grains, including: co-evaporated and annealed CZTSe at IBM (a) [2] John Wiley & Sons. (© 2014 WILEY-VCH Verlag GmbH & Co. KGaA, Weinheim), co-evaporated and annealed $Cu_2Zn(Sn,Ge)Se_4$ at AIST (b) (Reprinted from [51], Copyright (2016), with permission from Elsevier), co-evaporated CZTSe at NREL (c) [48] John Wiley & Sons. (Copyright © 2013 John Wiley & Sons, Ltd.), CZTSe:Ge prepared by metallic stack sputtering and annealing at IREC (d) (Reproduced from [6]. CC BY 3.0. © The Royal Society of Chemistry 2018), $Cu_2(Zn,Cd)SnS_4$ by co-sputtering of Cu/ZnS/SnS and annealing using CdS at USW (e) (Reprinted with permission from [114]. Copyright (2017) American Chemical Society), and co-sputtering of CZTS at ENEA (f) (Reprinted from [83], Copyright (2016), with permission from Elsevier.

very weak relationship with respect to the efficiency and V_{OC} [119]. The function and mechanism of the doping in single crystalline Si and GaAs are very simple. However, they are very complicated in quaternary CIGS and CZTS materials because the latter ones are basically used as polycrystalline and non-stoichiometric compounds. Therefore, more precise investigations are needed, especially in CZTS-based materials in order to understand the alkali role especially for higher conversion efficiency. It should be noted that alkali metals belong to group-I elements: they are expected to replace Cu (group I) sites in CIGS and CZTS. If the antisite defects, such as In_{Cu} or Zn_{Cu}, can be prevented by alkali doping, hole concentration can increase. On the contrary, if the Cu vacancy is replaced by an alkali element, hole concentration decreases.

For the pure sulfide compound, Bras *et al* studied the effect of sodium incorporation through sodium molybdate (MoNa) sputtered back contact in CZTS layers grown by sputtering from a compound target onto stainless steel substrates [120], demonstrating that Na-doped back contacts are compatible with a one-step sputtering process. The authors observed that sodium is needed to enhance recrystallization of CZTS layers, but surprisingly the MoNa layer thickness does not seem a critical parameter. Singh *et al* [121] reported sodium doping using NaF deposited onto CZTS layers grown by reactive sputtering of metal targets in H_2S, observing a significant grain growth and a shift of the optical bandgap from 1.45 eV (undoped) to 1.38 eV (with Na addition). On the other hand Yuan *et al* observed the expected 'U-like' sodium distribution along the thickness, with higher concentration at the interfaces in absorbers prepared by co-sputtering of metal precursors and further reactive annealing [122]. They did not observe a large impact on the morphology. Nevertheless, the efficiency of the resulting devices was relatively low. In this sense, a modest efficiency enhancement was observed by Sun *et al* by doping Cu, ZnS, and SnS co-sputtered precursors and then annealed under S atmosphere, using NaF as alkali source [123]. Finally, de la Cueva *et al* studied the Na doping of sulfurized co-evaporated CZTSe precursor (using Sn, Cu, ZnSe and Se sources, and NaF evaporated prior to the precursor deposition) [32]. The authors found a synergy between S incorporation and Na, where higher quantities of the alkali induce higher introduction levels of the chalcogen, showing improvement on the grain size and an increase of the carrier concentration.

In addition, Tampo *et al* found that the minority carrier lifetime is improved by Na doping in CZTSe. However, the efficiency improvement was found to be due to J_{SC} increase and not related to better V_{OC} values. This is explained by the fact that Na doping leads to a decrease of the carrier concentration in CZTSe, which corresponds to an increase of the Fermi level and a decrease of the built-in voltage of the PN junction. This built-in potential decrease is considered to cancel the suppression of recombination and the enhancement of lifetime. The surface recombination was found to also limit the minority carrier lifetime [124]. Tampo *et al* also showed V_{OC} limitation by surface recombinations, and demonstrated suppression of surface recombinations using surface oxidation [38]. The highest conversion efficiency of 11.7% in CZTSe solar was obtained by the combination of the surface treatment and the Na doping [38].

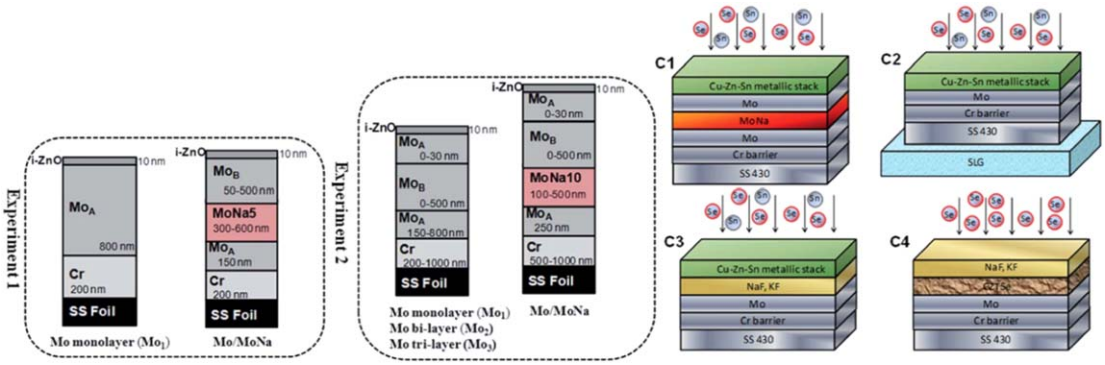

Figure 6. Different approaches investigated by Lopez-Marino *et al* for sodium doping of CZTSe. Reproduced from [125] with permission of The Royal Society of Chemistry.

Moreover, in the pure selenium compound, Lopez-Marino *et al* [125] investigated different approaches for alkali doping of sequential sputtering processed CZTSe, using flexible and alkali-free substrates as is shown in figure 6. In this work the authors observed important changes in both the surface morphology and the grain size of CZTSe mainly for Na doping. Two methodologies, the use of MoNa back contact and the pre-annealing synthesis doping using NaF, were identified as the most interesting methodologies, i.e. while post-deposition treatment with NaF is apparently useless for kesterites.

2.4.3. Alloying of kesterite for bandgap grading: S/Se, Zn/Cd and Ge/Sn

The main objective of kesterite alloying is to enable the tuning of the properties of the material for advanced device engineering. It is also viewed as a possible solution for intrinsic problems of kesterite absorbers like the Cu/Zn disorder or Sn-multivalency [126]. The most interesting alloying elements for kesterites are Ag replacing Cu, Cd replacing Zn, and Ge replacing Sn for cationic substitution, as well as Se replacing S for anionic substitution [126]. In principle, the introduction of all these elements in the basic kesterite structure can be performed by the PVD techniques described above and the monograin powder technology.

For example Ag-alloying has been successfully implemented by co-evaporation [127], Cd by co-sputtering or monograin growth process [114, 128], and Ge by co-evaporation, e-beam evaporation or monograin growth process [35, 51, 129]. On the other hand, the anionic substitution has been done by several approaches including selenization of one-step sputtered CZTS [66], selenization of sequentially sputtered CZTS [130], sulfo-selenization of sputtered metals [4, 56, 130, 131], or by single step PLD [132] and also by monograin growth process [95].

One of the main interests for developing alloying concepts using PVD processes is to demonstrate the possibility of bandgap gradients. If properly controlled, this can strongly help to reduce recombinations at the interfaces. Some attempts have been reported very recently using S/Se by Yang *et al* [4]. The authors demonstrated that the use of a hybrid chalcogenization via controlling the SeS_2/Se chalcogen sources weight ratios led to the possibility of obtaining decent graded bandgaps (see figures 7(a) and (b)). As presented in figure 7(c), bandgap grading in the depletion region allows a remarkable improvement of the conversion efficiency up to 12.3%.

With cations, there is still a lack of conclusive works, and only very recently the possibility to use Ge to introduce graded bandgap by substituting Sn has been demonstrated, however only for very low Ge quantities [133].

2.4.4. Kesterite submodules

In 2011, Solar Frontier reported the first kesterite-based submodule achieving an efficiency of 6.2% on a 5×5 cm^2 surface [134]. The submodule kesterite absorber layer was grown by sequential evaporation of precursors followed by sulfurization whereas the PN junction was obtained using the typical CdS buffer layer. As a part of the effort for CRM-free technologies, Hiroi *et al* also reported a first In, Se and Cd free kesterite-based submodule resulting in an efficiency of 2.0% on an area of 5×5 cm^2. Since then, Solar Frontier continuously increased their kesterite-based submodules efficiency by reporting in 2012, values of 6.3% and 5.8% with respectively In-based and Zn-based buffer layers. Those efficiencies were obtained thanks to the optimization of the pre-treatment of the buffer layer deposited via chemical bath process [135]. In the same year, thanks to the

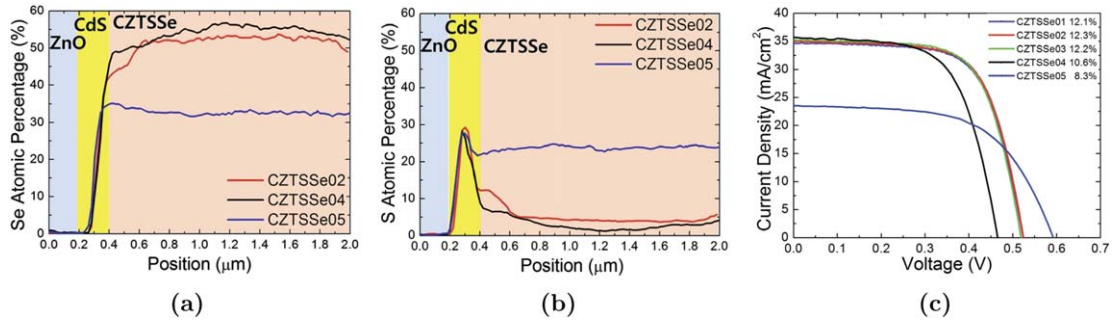

Figure 7. Selenium (a) and sulfur (b) depth profiles obtained using STEM-EDS measurements in CZTSSe absorber layers grown by chalcogenization with different SeS_2/Se chalcogen sources weight ratios. (c) Current density–voltage characteristics of the corresponding CZTSSe solar cells. Reproduced from [4] with permission of The Royal Society of Chemistry.

optimization of the CZTS absorber thin film uniformity and thickness, an efficiency of 8.6% was achieved using a CdS buffer layer [136]. The authors reported that a 600 nm thick absorber should be sufficient to ensure optimal light absorption and observed a remarkable improvement of the V_{OC} for an ultrathin layer with flattened surface. More recently, in 2014, Solar Frontier reported an efficiency of 11.0% by introducing a bandgap gradient within the absorber layer. This result was obtained despite the decrease of the *FF* due to ZnS segregation at the rear interface reported by the authors [8, 17]. In addition, a 14 cm^2 CZTS sputtered submodule was reported to achieve an efficiency of 6.34% [17].

3. Summary

Over the last years, the main issue concerning kesterite thin films for solar cell applications was focused on the device efficiency, a concern that has to be distinguished from issues related to large-scale applications. As soon as the power conversion has reached competitive levels, kesterite materials will demonstrate promising results for future investigations and applications. Nowadays, high kesterite-based cell efficiency enhancements have been reported thanks to the evolution of the physical vapor deposition procedures used for the synthesis of the absorber layer. Now used as a benchmark process, two-step kesterite synthesis, namely low temperature deposition of elemental precursors followed by sulfurization/selenization treatment, have demonstrated devices with comparable efficiencies than those reported by chemical routes thanks to a better control of the grain growth and the limitation of Sn(S,Se) losses and secondary phases formation. These elemental losses are known to cause a V_{OC} deficit through the formation of deep defects within the bandgap. Using sputtering routes, the optimization of the synthesis procedure through the elucidation and the control of the reaction pathway by using Cu–Sn target allows to minimize Sn(S,Se) losses during annealing treatment. The sequential sputtering route was optimized through investigations of the stacking order and the thicknesses of deposited precursors, leading to better adhesion of the absorber layer, reduction of element losses and reduction of voids density at the rear interface. Several improvements were also achieved thanks to the optimization of the annealing procedure using Sn addition during the annealing to reduce the Sn(S,Se) losses. In the case of pure sulfide CZTS solar cells, the use of a combined S and SnS atmosphere during the sulfurization of co-sputtered precursors was also demonstrated to promote the formation of an improved CZTS/CdS front interface, leading to an efficiency enhancement, reaching the record of 11%. Concerning CZTSSe-based cell, the highest efficiency of 12.6% has been achieved using H_2S and Se atmosphere and highlighting the impact of the right precursor stacking on the absorber layer performances. On the other hand, using PLD route, the optimization of the laser fluence was reported to be mandatory to obtain the right thin film stoichiometry. Concerning monograin growth processes, the optimization of post-treatments of crystal surfaces by chemical etching and annealing in chalcogenide-containing atmosphere leads to improvements of the crystal surface composition. It is worth mentioning that efficiency progresses cannot simply be ascribed to the optimization of the absorber layer synthesis procedures alone. Indeed, beneficial effects from PDA, buffer layer optimization and interfaces passivation have also contributed to the solar cell efficiency enhancement over the years. Finally, compared to CVD processes, the synthesis of kesterite absorber layers using PVD routes offers safer (as far as environmental issues are concerned) and more reproducible scale-up procedures and is beneficial in terms of high throughput. In addition, alkali doping and alloying both promise efficiency enhancements as future perspectives for CZT(S,Se) solar cells. Through this paper, the focus has been put on the status overview of the physical routes used for the synthesis of

kesterite. Complementary aspects related to theoretical and experimental investigations of kesterite materials can be found in the corresponding contributions of this journal issue.

Acknowledgments

1. R Caballero and M León acknowledge financial support via the Spanish Ministry of Science, Innovation and Universities project (WINCOST, ENE2016-80788-C5-2-R) and thank H2020 EU Programme under the project INFINITE-CELL (H2020-MSCA-RISE-2017-777968).
2. S Canulescu and J Schou acknowledge the support from Innovation Fund Denmark.
3. D-H Kim acknowledges financial support via the DGIST R&D Program of the Ministry of Science and ICT, KOREA (18-BD-05).
4. C Malerba acknowledges the support from the Italian Ministry of Economic Development in the framework of the Operating Agreement with ENEA for the Research on the Electric System.
5. A Redinger acknowledges financial support via the FNR Attract program, Project : SUNSPOT, Nr. 11244141.
6. E Saucedo thanks H2020 EU Programme under the projects STARCELL (H2020-NMBP-03-2016-720907) and INFINITE-CELL (H2020-MSCA-RISE-2017-777968), the Spanish Ministry of Science, Innovation and Universities for the IGNITE project (ENE2017-87671-C3-1-R), and the European Regional Development Funds (ERDF, FEDER Programa Competitivitat de Catalunya 2007–2013). IREC belong to the SEMS (Solar Energy Materials and Systems) Consolidated Research Group of the 'Generalitat de Catalunya' (Ref. 2017 SGR 862).
7. Taltech acknowledges financial support via the Estonian Ministry of Education and Research funding project IUT19-28 and the European Union Regional Development Fund, Project TK141.
8. B Vermang has received funding from the European Research Council (ERC) under the European Union's Horizon 2020 Research and Innovation Programme (Grant Agreement No 715027).

ORCID iDs

T Ratz https://orcid.org/0000-0002-3629-1087
G Brammertz https://orcid.org/0000-0003-1404-7339
R Caballero https://orcid.org/0000-0003-0215-7311
S Canulescu https://orcid.org/0000-0003-3786-2598
J Schou https://orcid.org/0000-0002-8647-2679
L Gütay https://orcid.org/0000-0002-7626-8586
D Pareek https://orcid.org/0000-0001-7231-6686
D-H Kim https://orcid.org/0000-0002-8580-1629
C Malerba https://orcid.org/0000-0001-6976-3442
E Saucedo https://orcid.org/0000-0003-2123-6162
H Tampo https://orcid.org/0000-0002-6666-0285
K Timmo https://orcid.org/0000-0001-6054-6783
N D Nguyen https://orcid.org/0000-0002-0142-1611
B Vermang https://orcid.org/0000-0003-2669-2087

References

[1] PV Magazine 2019 Solar Frontier hits new CIS cell efficiency record, www.solar-frontier.com/eng/news/2019/0117_press.html (accessed 14 February 2019)
[2] Lee Y S *et al* 2015 $Cu_2ZnSnSe_4$ thin-film solar cells by thermal Co-evaporation with 11.6% efficiency and improved minority carrier diffusion length *Adv. Energy Mater.* **5** 1401372
[3] Kim S, Kim K M, Tampo H, Shibata H and Niki S 2016 Improvement of voltage deficit of Ge-incorporated kesterite solar cell with 12.3% conversion efficiency *Appl. Phys. Express* **9** 102301
[4] Yang K-J *et al* 2016 A band-gap-graded CZTSSe solar cell with 12.3% efficiency *J. Mater. Chem.* A **4** 10151
[5] Yan C *et al* 2018 Cu_2ZnSnS_4 solar cells with over 10% power conversion efficiency enabled by heterojunction heat treatment *Nat. Energy* **3** 764–72
[6] Giraldo S *et al* 2018 How small amounts of Ge modify the formation pathways and crystallization of kesterites *Energy Environ. Sci.* **11** 582

[7] Green M A *et al* 2018 Solar cell efficiency tables (Version 53) *Prog. Photovolt. Res. Appl.* **27** 3
[8] Kato T, Sakai N and Sugimoto H 2014 Efficiency improvement of $Cu_2ZnSn(S,Se)_4$ submodule with graded bandgap and reduced backside ZnS segregation *2014 IEEE 40th Photovoltaic Specialist Conf. (PVSC)* (Piscataway, NJ : IEEE) pp 0844–6
[9] Taskesen T *et al* 2018 Device characteristics of an 11.4% CZTSe solar cell fabricated from sputtered precursors *Adv. Energy Mater.* **8** 1703295
[10] Son D-H *et al* 2018 *Rep. 9th Eur. Kesterite Work (Ghent)*
[11] *Communication from the commission to the European parliament, the council, the European economic and social committee and the committee of the regions on the 2017 list of Critical Raw Materials for the EU*, https://eur-lex.europa.eu/legal-content/EN/ALL/?uri=COM:2017:0490:FIN (accessed 14 February 2017).
[12] Lopez-Marino S *et al* 2016 The importance of back contact modification in $Cu_2ZnSnSe_4$ solar cells: the role of a thin MoO_2 layer *Nano Energy* **26** 708
[13] Wada T, Kohara N, Nishiwaki S and Negami T 2001 Characterization of the $Cu(In,Ga)Se_2$/Mo interface in CIGS solar cells *Thin Solid Films* **387** 118
[14] Wang W *et al* 2013 Device characteristics of CZTSSe thin-film solar cells with 12.6% efficiency *Adv. Energy Mater.* **4** 1301465
[15] Katagiri H *et al* 2008 Enhanced conversion efficiencies of Cu_2ZnSnS_4-based thin film solar cells by using preferential etching technique *Appl. Phys. Express* **1** 041201
[16] Shin B *et al* 2013 Thin film solar cell with 8.4% power conversion efficiency using an earth-abundant Cu_2ZnSnS_4 absorber *Prog. Photovolt. Res. Appl.* **21** 72
[17] Hiroi H, Sakai N, Kato T and Sugimoto H 2013 High voltage Cu_2ZnSnS_4 submodules by hybrid buffer layer *2013 IEEE 39th Photovoltaic Specialists Conf. (PVSC)* (Piscataway, NJ: IEEE) pp 0863–6
[18] Scragg J J *et al* 2013 Effects of back contact instability on Cu_2ZnSnS_4 devices and processes *Chem. Mater.* **25** 3162
[19] Yang K-J *et al* 2015 Effects of the compositional ratio distribution with sulfurization temperatures in the absorber layer on the defect and surface electrical characteristics of Cu_2ZnSnS_4 solar cells *Prog. Photovolt. Res. Appl.* **23** 1771
[20] Kauk-Kuusik M *et al* 2015 PN junction improvements of Cu_2ZnSnS_4/CdS monograin layer solar cells *Appl. Surf. Sci.* **357** 795
[21] Sun K *et al* 2016 Over 9% efficient kesterite Cu_2ZnSnS_4 solar cell fabricated by using $Zn_{1-x}Cd_xS$ buffer layer *Adv. Energy Mater.* **6** 1600046
[22] Feng Y *et al* 2016 A low-temperature formation path toward highly efficient Se-free Cu_2ZnSnS_4 solar cells fabricated through sputtering and sulfurization *CrystEngComm* **18** 1070
[23] Ericson T *et al* 2017 Zinc-tin-oxide buffer layer and low temperature post annealing resulting in a 9.0% efficient Cd-Free Cu_2ZnSnS_4 solar cell *Solar RRL* **1** 1700001
[24] Malerba C, Valentini M and Mittiga A 2017 Cation disorder in Cu_2ZnSnS_4 thin films: effect on solar cell performances *Solar RRL* **1** 1700101
[25] Cazzaniga A *et al* 2017 Ultra-thin Cu_2ZnSnS_4 solar cell by pulsed laser deposition *Sol. Energy Mater. Sol. Cells* **166** 91
[26] Timmo K *et al* 2017 Influence of order-disorder in Cu_2ZnSnS_4 powders on the performance of monograin layer solar cells *Thin Solid Films* **633** 122
[27] Gansukh M *et al* 2019 Oxide route for Cu_2ZnSnS_4 solar cells by pulsed laser deposition *46th IEEE PVSC*
[28] Redinger A, Berg D M, Dale P J and Siebentritt S 2011 The consequences of kesterite equilibria for efficient solar cells *J. Am. Chem. Soc.* **133** 3320
[29] Repins I *et al* 2012 Co-evaporated $Cu_2ZnSnSe_4$ films and devices *Sol. Energy Mater. Sol. Cells* **101** 154
[30] Redinger A *et al* 2014 Different bandgaps in $Cu_2ZnSnSe_4$: a high temperature coevaporation study *IEEE J. Photovolt.* **5** 641
[31] Larsen J K *et al* 2017 Surface modification through air annealing $Cu_2ZnSn(S,Se)_4$ absorbers *Thin Solid Films* **633** 118
[32] de la Cueva L *et al* 2018 Sulfurization of co-evaporated $Cu_2ZnSnSe_4$ thin film solar cells The role of Na *Sol. Energy Mater. Sol. Cells* **186** 115
[33] Neubauer C, Samieipour A, Oueslati S, Ernits K and Meissner D 2018 Spatially resolved opto-electrical performance investigations of $Cu_2ZnSnS_{3.2}Se_{0.8}$ photovoltaic devices *Energy Sci. Eng.* **6** 563
[34] Buffière M *et al* 2015 Physical characterization of $Cu_2ZnGeSe_4$ thin films from annealing of Cu–Zn–Ge precursor layers *Thin Solid Films* **582** 171
[35] Choubrac L *et al* 2018 7.6% CZGSe solar cells thanks to optimized CdS chemical bath deposition *Phys. Status Solidi* a **215** 1800043
[36] Taskesen T *et al* 2018 Resilient and reproducible processing for CZTSe solar cells in the range of 10% *Prog. Photovolt. Res. Appl.* **26** 1003
[37] Sun R *et al* 2018 Beyond 11% efficient $Cu_2ZnSn(Se,S)_4$ thin film solar cells by cadmium alloying *Sol. Energy Mater. Sol. Cells* **174** 494
[38] Tampo H, Kim S, Nagai T, Shibata H and Niki S 2019 Improving the open circuit voltage through surface oxygen plasma treatment and 11.7% efficient $Cu_2ZnSnSe_4$ solar cell *ACS Appl. Mater. Interfaces* **11** 13319–25
[39] Green M A, Hishikawa Y, Dunlop E D, Levi D H, Hohl-Ebinger J and Ho-Baillie A W 2018 Solar cell efficiency tables (version 52) *Prog. Photovolt., Res. Appl.* **26** 427–36
[40] Chirilă A *et al* 2011 Highly efficient $Cu(In,Ga)Se_2$ solar cells grown on flexible polymer films *Nat. Mater.* **10** 857
[41] Gabor A M *et al* 1994 High-efficiency $CuIn_xGa_{1-x})Se_2$ solar cells made from $(In_x,Ga_{1-x})_2Se_3$ precursor films *Appl. Phys. Lett.* **65** 198
[42] Witte W *et al* 2014 Gallium gradients in $Cu(In,Ga)Se_2$ thin-film solar cells *Prog. Photovolt. Res. Appl.* **23** 717
[43] Sakurai K *et al* 2004 In situ diagnostic methods for thin-film fabrication: utilization of heat radiation and light scattering *Prog. Photovolt. Res. Appl.* **12** 219
[44] Kaufmann C A, Neisser A, Klenk R and Scheer R 2005 Transfer of $Cu(In,Ga)Se_2$ thin film solar cells to flexible substrates using an *in situ* process control *Thin Solid Films* **480** 515
[45] Caballero R *et al* 2011 Investigation of $Cu(In,Ga)Se_2$ thin-film formation during the multi-stage co-evaporation process *Prog. Photovolt. Res. Appl.* **21** 30
[46] Weber A *et al* 2009 Multi-stage evaporation of Cu_2ZnSnS_4 thin films *Thin Solid Films* **517** 2524
[47] Schubert B-A *et al* 2011 Cu_2ZnSnS_4 thin film solar cells by fast coevaporation *Prog. Photovolt. Res. Appl.* **19** 93
[48] Hsu W-C *et al* 2013 Growth mechanisms of co-evaporated kesterite: a comparison of Cu-rich and Zn-rich composition paths *Prog. Photovolt. Res. Appl.* **22** 35
[49] Redinger A *et al* 2011 Detection of a ZnSe secondary phase in coevaporated $Cu_2ZnSnSe_4$ thin films *Appl. Phys. Lett.* **98** 101907
[50] Choi S G *et al* 2014 Temperature dependent band-gap energy for $Cu_2ZnSnSe_4$. A spectroscopic ellipsometric study *Sol. Energy Mater. Sol. Cells* **130** 375
[51] Kim S *et al* 2016 Ge-incorporated $Cu_2ZnSnSe_4$ thin-film solar cells with efficiency greater than 10% *Sol. Energy Mater. Sol. Cells* **144** 488

[52] Rey G *et al* 2016 Ordering kesterite improves solar cells: a low temperature post-deposition annealing study *Sol. Energy Mater. Sol. Cells* **151** 131
[53] Kim J, Park S, Ryu S, Oh J and Shin B 2017 Improving the open-circuit voltage of $Cu_2ZnSnSe_4$ thin film solar cells via interface passivation *Prog. Photovolt. Res. Appl.* **25** 308
[54] Antunez P D *et al* 2017 Back contact engineering for increased performance in kesterite solar cells *Adv. Energy Mater.* **7** 1602585
[55] Fairbrother A *et al* 2013 On the formation mechanisms of Zn-rich Cu_2ZnSnS_4 films prepared by sulfurization of metallic stacks *Sol. Energy Mater. Sol. Cells* **112** 97
[56] Fairbrother A *et al* 2013 Single-step sulfo-selenization method to synthesize $Cu_2ZnSn(S_ySe_{1-y})_4$ absorbers from metallic stack precursors *ChemPhysChem* **14** 1836
[57] Giraldo S *et al* 2016 $Cu_2ZnSnSe_4$-based solar cells with efficiency exceeding 10% by adding a superficial Ge nanolayer: the interaction between Ge and Na *IEEE J. Photovolt.* **6** 754
[58] Yoo H and Kim J 2010 Growth of Cu_2ZnSnS_4 thin films using sulfurization of stacked metallic films *Thin Solid Films* **518** 6567
[59] Fernandes P A, Salome P M P, da Cunha A F and Schubert B-A 2011 Cu_2ZnSnS_4 solar cells prepared with sulphurized DC-sputtered stacked metallic precursors *Thin Solid Films* **519** 7382
[60] Ge J *et al* 2012 Fabrication of Cu_2ZnSnS_4 absorbers by sulfurization of Sn-rich precursors *Phys. Status Solidi* a **209** 1493
[61] Guo H *et al* 2018 The fabrication of Cd-free Cu_2ZnSnS_4-Ag_2ZnSnS_4 heterojunction photovoltaic devices *Sol. Energy Mater. Sol. Cells* **178** 146
[62] Oo W H *et al* 2011 Grain size and texture of Cu_2ZnSnS_4 thin films synthesized by cosputtering binary sulfides and annealing: effects of processing conditions and sodium *J. Electron. Mater.* **40** 2214
[63] Liu F *et al* 2017 Beyond 8% ultrathin kesterite Cu_2ZnSnS_4 solar cells by interface reaction route controlling and self-organized nanopattern at the back contact *NPG Asia Mater.* **9** e401
[64] Ericson T, Scragg J J, Kubart T, Törndahl T and Platzer-Björkman C 2013 Annealing behavior of reactively sputtered precursor films for Cu_2ZnSnS_4 solar cells *Thin Solid Films* **535** 22
[65] Brammertz G *et al* 2013 Correlation between physical, electrical, and optical properties of $Cu_2ZnSnSe_4$ based solar cells *Appl. Phys. Lett.* **102** 013902
[66] Lin Y-P, Hsieh T-E, Chen Y-C and Huang K-P 2017 Characteristics of $Cu_2ZnSn(S_xSe_{1-x})_4$ thin-film solar cells prepared by sputtering deposition using single quaternary Cu_2ZnSnS_4 target followed by selenization/sulfurization treatment *Sol. Energy Mater. Sol. Cells* **162** 55
[67] Nakamura R *et al* 2014 Cu_2ZnSnS_4 thin film deposited by sputtering with Cu_2ZnSnS_4 compound target *Japan. J. Appl. Phys.* **53** 02BC10
[68] Shimada T *et al* 2007 Cu2ZnSnS4 thin film solar cells prepared from sputtered and evaporated precursors *International Symposiumon Organic and Inorganic Electronic Materials and Related Nanotechnologies (19 - 22 June)* 162
[69] Brammertz G *et al* 2013 Electrical characterization of $Cu_2ZnSnSe_4$ solar cells from selenization of sputtered metal layers *Thin Solid Films* **535** 348
[70] Brammertz G *et al* 2013 Characterization of defects in 9.7% efficient $Cu_2ZnSnSe_4$-CdS-ZnO solar cells *Appl. Phys. Lett.* **103** 163904
[71] Son D H *et al* 2015 Growth and device characteristics of CZTSSe thin-film solar cells with 8.03% efficiency *Chem. Mater.* **27** 5180
[72] Kim S-Y *et al* 2019 Void and secondary phase formation mechanisms of CZTSSe using Sn/Cu/Zn/Mo stacked elemental precursors *Nano Energy* **59** 399
[73] Chawla V and Clemens B 2012 Effect of composition on high efficiency CZTSSe devices fabricated using co-sputtering of compound targets *2012 38th IEEE Photovoltaic Specialists Conf.* (Piscataway, NJ: IEEE) 002990
[74] Andres C, Haass S, Romanyuk Y and Tiwari A 2017 9.4% efficient $Cu_2ZnSnSe_4$ solar cells from co-sputtered elemental metal precursor and rapid thermal annealing *Thin Solid Films* **633** 141
[75] Bodeux R, Mollica F and Delbos S 2015 Growth of $Cu_2ZnSnSe_4$ by cosputtering and reactive annealing atmosphere *Sol. Energy Mater. Sol. Cells* **132** 67
[76] Scragg J J *et al* 2013 Effects of back contact instability on Cu_2ZnSnS_4 devices and processes *Chem. Mater.* **25** 3162
[77] Englund S, Saini N and Platzer-Björkman C 2018 $Cu_2ZnSn(S,Se)_4$ from annealing of compound co-sputtered precursors: recent results and open questions *Sol. Energy* **175** 84
[78] Yan C *et al* 2016 Boosting the efficiency of pure sulfide CZTS solar cells using the In/Cd-based hybrid buffers *Sol. Energy Mater. Sol. Cells* **144** 700
[79] Santoni A *et al* 2013 Valence band offset at the CdS/Cu_2ZnSnS_4 interface probed by x-ray photoelectron spectroscopy *J. Phys. D: Appl. Phys.* **46** 175101
[80] Bär M *et al* 2011 Cliff-like conduction band offset and KCN-induced recombination barrier enhancement at the CdS/Cu_2ZnSnS_4 thin-film solar cell heterojunction *Appl. Phys. Lett.* **99** 222105
[81] Liu F *et al* 2016 Nanoscale microstructure and chemistry of Cu_2ZnSnS_4/CdS interface in kesterite Cu_2ZnSnS_4 solar cells *Adv. Energy Mater.* **6** 1600706
[82] Ericson T, Scragg J J, Kubart T, Törndahl T and Platzer-Björkman C 2013 Annealing behavior of reactively sputtered precursor films for Cu_2ZnSnS_4 solar cells *Thin Solid Films* **535** 22
[83] Malerba C *et al* 2016 Blistering in Cu_2ZnSnS_4 thin films: correlation with residual stresses *Mater. Des.* **108** 725
[84] Liu F *et al* 2016 Nanoscale microstructure and chemistry of Cu_2ZnSnS_4/CdS interface in kesterite Cu_2ZnSnS_4 solar cells *Adv. Energy Mater.* **6** 1600706
[85] Moriya K, Tanaka K and Uchiki H 2007 Fabrication of Cu_2ZnSnS_4 thin-film solar cell prepared by pulsed laser deposition *Japan. J. Appl. Phys.* **46** 5780
[86] Ettlinger R B, Cazzaniga A, Canulescu S, Pryds N and Schou J 2015 Pulsed laser deposition from ZnS and Cu_2SnS_3 multicomponent targets *Appl. Surf. Sci.* **336** 385
[87] Vanalakar S A *et al* 2015 Fabrication of Cu_2SnS_3 thin film solar cells using pulsed laser deposition technique *Sol. Energy Mater. Sol. Cells* **138** 1
[88] Sulaiman N S C, Nee C H, Yap S L, Lee Y S, Tou T Y and Yap S S 2015 The growth of nanostructured Cu_2ZnSnS_4 films by pulsed laser deposition *Appl. Surf. Sci.* **354** 42–47
[89] Vanalakar S A *et al* 2015 A review on pulsed laser deposited CZTS thin films for solar cell applications *J. Alloys Compd.* **619** 109
[90] Schou J *et al* 2018 Pulsed laser deposition of chalcogenide sulfides from multi- and single-component targets: the non-stoichiometric material transfer *Appl. Phys.* A **124** 78
[91] Jin X *et al* 2016 Pulsed laser deposition of $Cu_2ZnSn(S_xSe_{(1-x)})_4$ thin film solar cells using quaternary oxide target prepared by combustion method *Sol. Energy Mater. Sol. Cells* **155** 216

[92] Altosaar M *et al* 2006 $Cu_2ZnSnSe_4$ monograin powder for solar cell application *Conf. Record of the 2006 IEEE 4th World Conf. on Photovoltaic Energy Conversion (Waikoloa, HI, 07–12 May)* (IEEE Electron Devices Society) 468
[93] Altosaar M *et al* 2008 $Cu_2Zn_{1-x}Cd_xSn(Se_{1-y}S_y)_4$ solid solutions as absorber materials for solar cells *Phys. Status Solidi* a **205** 167
[94] Grossberg M, Krustok J, Timmo K and Altosaar M 2009 Radiative recombination in $Cu_2ZnSnSe_4$ monograins studied by photoluminescence spectroscopy *Thin Solid Films* **517** 2489
[95] Timmo K *et al* 2010 Sulfur-containing $Cu_2ZnSnSe_4$ monograin powders for solar cells *Sol. Energy Mater. Sol. Cells* **94** 1889
[96] Grossberg M *et al* 2011 Photoluminescence and Raman study of $Cu_2ZnSn(Se_xS_{1-x})_4$ monograins for photovoltaic applications *Thin Solid Films* **519** 7403
[97] Danilson M *et al* 2011 XPS study of CZTSSe monograin powders *Thin Solid Films* **519** 7407
[98] Timmo K *et al* 2010 Chemical etching of $Cu_2ZnSn(S,Se)_4$ monograin powder *2010 35th IEEE Photovoltaic Specialists Conf.* (Piscataway, NJ : IEEE) 001982
[99] Kauk M *et al* 2011 Effects of sulphur and tin disulphide vapour treatments of $Cu_2ZnSnS(Se)_4$ absorber materials for monograin solar cells *Energy Proc.* **10** 197
[100] Klinkert T *et al* 2016 New insights into the Mo/Cu(In,Ga)Se_2 interface in thin film solar cells: formation and properties of the $MoSe_2$ interfacial layer *J. Chem. Phys.* **145** 154702
[101] Kim S, Oh M and Kim W K 2013 Effect of Sn-layer addition to precursors on characteristics of $Cu_2ZnSn(S,Se)_4$ thin-film solar cell absorber *Thin Solid Films* **549** 59
[102] Yin X *et al* 2015 Significantly different mechanical properties and interfacial structures of $Cu_2ZnSn(S,Se)_4$ films prepared from metallic and sulfur-contained precursors *Sol. Energy Mater. Sol. Cells* **134** 389
[103] López-Marino S *et al* 2013 Inhibiting the absorber/Mo-back contact decomposition reaction in $Cu_2ZnSnSe_4$ solar cells: the role of a ZnO intermediate nanolayer *J. Mater. Chem.* A **1** 8338
[104] Yan C *et al* 2017 Boost V_{OC} of pure sulfide kesterite solar cell via a double CZTS layer stacks *Sol. Energy Mater. Sol. Cells* **160** 7
[105] Thersleff T *et al* 2017 Chemically and morphologically distinct grain boundaries in Ge-doped $Cu_2ZnSnSe_4$ solar cells revealed with STEM-EELS *Mater. Des.* **122** 102–9
[106] Hwang S *et al* 2015 Effects of a pre-annealing treatment (PAT) on $Cu_2ZnSn(S,Se)_4$ thin films prepared by rapid thermal processing (RTP) selenization *Sol. Energy Mater. Sol. Cells* **143** 218
[107] Wei Y *et al* 2018 Effects of selenium atmosphere on grain growth for CZTSe absorbers fabricated by selenization of as-sputtered precursors *J. Alloys Compd.* **755** 224
[108] Abusnina M *et al* 2015 *IEEE 42nd Photovolt. Spec. Conf.* p 1
[109] López-Marino S *et al* 2013 Inhibiting the absorber/Mo-back contact decomposition reaction in $Cu_2ZnSnSe_4$ solar cells: the role of a ZnO intermediate nanolayer *J. Mater. Chem.* A **1** 8338
[110] Zhuk S *et al* 2019 Effect of TaN intermediate layer on the back contact reaction of sputter-deposited Cu poor Cu_2ZnSnS_4 and Mo *Appl. Surf. Sci.* **471** 277
[111] Guo H *et al* 2018 Dual function of ultrathin Ti intermediate layers in CZTS solar cells Sulfur blocking and charge enhancement *Sol. Energy Mater. Sol. Cells* **175** 20
[112] Giraldo S *et al* 2016 $Cu_2ZnSnSe_4$ solar cells with 10.6% efficiency through innovative absorber engineering with Ge superficial nanolayer *Prog. Photovolt. Res. Appl.* **24** 1359
[113] Giraldo S *et al* 2015 Large efficiency improvement in $Cu_2ZnSnSe_4$ solar cells by introducing a superficial Ge nanolayer *Adv. Energy Mater.* **5** 1501070
[114] Yan C *et al* 2017 Beyond 11% efficient sulfide kesterite $Cu_2Zn_xCd_{1-x}SnS_4$ solar cell: effects of cadmium alloying *ACS Energy Lett.* **2** 930
[115] Romeo A *et al* 2004 Development of thin-film Cu(In,Ga)Se_2 and CdTe solar cells *Prog. Photovolt. Res. Appl.* **12** 93
[116] Jackson P *et al* 2016 Effects of heavy alkali elements in Cu(In,Ga)Se_2 solar cells with efficiencies up to 22.6% *Phys. Status Solidi* **10** 583
[117] Kato T, Wu J-L, Hirai Y, Sugimoto H and Bermudez V 2019 Record efficiency for thin-film polycrystalline solar cells up to 22.9%; achieved by Cs-Treated Cu(In,Ga)$(Se,S)_2$ *IEEE J. Photovolt.* **9** 325
[118] Sutter-Fella C M *et al* 2014 Sodium assisted sintering of chalcogenides and its application to solution processed $Cu_2ZnSn(S,Se)_4$ thin film solar cells *Chem. Mater.* **26** 1420
[119] Hages C J *et al* 2017 Identifying the real minority carrier lifetime in nonideal semiconductors: a case study of kesterite materials *Adv. Energy Mater.* **7** 1700167
[120] Bras P, Sterner J and Platzer-Björkman C 2015 Influence of hydrogen sulfide annealing on copper-zinc-tin-sulfide solar cells sputtered from a quaternary compound target *Thin Solid Films* **582** 233
[121] Singh O P, Gour K S, Parmar R and Singh V N 2016 Sodium induced grain growth, defect passivation and enhancement in the photovoltaic properties of Cu_2ZnSnS_4 thin film solar cell *Mater. Chem. Phys.* **177** 293
[122] Yuan L *et al* 2016 Investigation of sodium distribution in CuZnSnS thin films and its effects on the performance of the solar cells *Mater. Res. Bull.* **84** 314
[123] Sun K *et al* 2016 Influence of sodium incorporation on kesterite Cu_2ZnSnS_4 solar cells fabricated on stainless steel substrates *Sol. Energy Mater. Sol. Cells* **157** 565
[124] Tampo H, Kim K M, Kim S, Shibata H and Niki S 2017 Improvement of minority carrier lifetime and conversion efficiency by Na incorporation in $Cu_2ZnSnSe_4$ solar cells *J. Appl. Phys.* **122** 023106
[125] López-Marino S *et al* 2016 Alkali doping strategies for flexible and light-weight $Cu_2ZnSnSe_4$ solar cells *J. Mater. Chem.* A **4** 1895
[126] Giraldo S *et al* 2019 Progress and perspectives of thin film kesterite photovoltaic technology: a critical review *Adv. Mater.* **43** 1806692
[127] Gershon T *et al* 2016 Photovoltaic materials and devices based on the alloyed kesterite absorber $(Ag_xCu_{1-x})_2ZnSnSe_4$ *Adv. Energy Mater.* **6** 1502468
[128] Pilvet M *et al* 2015 Compositionally tunable structure and optical properties of $Cu_{1.85}(Cd_xZn_{1-x})_{1.1}SnS_{4.1}$ $(0 < x < 1)$ monograin powders *Thin Solid Films* **582** 180–3
[129] Oueslati S *et al* 2019 Effect of germanium incorporation on the properties of kesterite $Cu_2ZnSn(S,Se)_4$ monograins *Thin Solid Films* **669** 315
[130] Kim J *et al* 2018 High photo-conversion efficiency $Cu_2ZnSn(S,Se)_4$ thin-film solar cells prepared by compound-precursors and metal-precursors *Sol. Energy Mater. Sol. Cells* **183** 129
[131] Xie H *et al* 2015 Formation and impact of secondary phases in Cu-poor Zn-rich $Cu_2ZnSn(S_{1-y}Se_y)_4$ $(0 \leqslant y \leqslant 1)$ based solar cells *Sol. Energy Mater. Sol. Cells* **140** 289
[132] He J *et al* 2012 Single-step preparation and characterization of $Cu_2ZnSn(S_xSe_{1-x})_4$ thin films deposited by pulsed laser deposition method *J. Alloys Compd.* **529** 34

[133] Marquez J *et al* 2017 Chemistry and dynamics of Ge in kesterite: toward band-gap-graded absorbers *Chem. Mater.* **29** 9399
[134] Hiroi H, Sakai N and Sugimoto H 2011 Cd-free 5 × 5cm^2-sized Cu_2ZnSnS_4 submodules *2011 37th IEEE Photovoltaic Specialists Conf.* (Piscataway, NJ: IEEE) pp 002719–22
[135] Hiroi H, Sakai N, Muraoka S, Katou T and Sugimoto H 2012 Development of high efficiency Cu_2ZnSnS_4 submodule with Cd-free buffer layer *2012 38th IEEE Photovoltaic Specialists Conf.* (Piscataway, NJ: IEEE) 001811
[136] Sugimoto H, Hiroi H, Sakai N, Muraoka S and Katou T 2012 Over 8% efficiency Cu_2ZnSnS_4 submodules with ultra-thin absorber *2012 38th IEEE Photovoltaic Specialists Conf.* (Piscataway, NJ: IEEE) 002997